

A steady-state electrical model of a microbial fuel cell through multiple-cycle polarization curves

P.M.D. Serra ^{a,*}, A. Espírito-Santo ^a, M. Magrinho ^b

^a Department of Electromechanical Engineering and Instituto de Telecomunicações, University of Beira Interior, Covilhã, 6201-001, Portugal

^b Department of Chemistry, University of Beira Interior, Covilhã, 6201-001, Portugal



ARTICLE INFO

Keywords:

Microbial fuel cells
Energy harvesting
Electrical model
Internal resistance
Maximum power

ABSTRACT

The use of Microbial Fuel Cells as power sources in rural or remote locations can solve issues related with power availability and wastewater cleaning. Furthermore, the application of such technology in wireless smart sensors applied to wastewater treatment plants can also help in water quality monitoring, increasing the process autonomy and reliability. A trustworthy power source needs to have a predictable and repeatable behavior, which cannot be achieved without adequate models and supporting hardware for energy regulation and storage. The work herein described proposes a steady-state model, represented by an electric circuit made of passive components. This model was first applied to a specific 28 mL air-cathode Microbial Fuel Cells working with artificial wastewater and using graphite brush anodes. Afterwards, the model was further validated by applying it to a larger reactor and to other bibliographic records. The goal of the study is to propose a method for finding a Microbial Fuel Cell model to be used with maximum power point tracking research, guaranteeing the best-case scenario for Microbial Fuel Cell operation as a power source. The reactors used in this study were analyzed by relating time and voltage development, both in colonization and in polarization studies. A mathematical relationship model was developed and proposed allowing to separate MFC's behavior, concerning energy production, in to meaningful components. From the experimental data the method was used to obtain a two-component circuit model that describes the power behavior of this specific Microbial Fuel Cell topology. The same method can be used to described other MFC.

1. Introduction

Electric energy availability in rural and remote locations is very different from that in cities and urban settings, due to distance and investment unbalances. Having the ability to increase that energy availability without the need to install large infrastructures or to change landscapes or water flow is of particular interest, namely in the current context of environmental concerns. Typically, wastewater treatment facilities share the same energy challenges as those from rural and remote locations, which, in turn, highlights the applicability and usefulness, particularly to limit the energy consumption, of low power wireless network smart sensors [1]. This monitoring solution can address power outflows for water monitoring and stream control. Existing smart sensors have their biggest limitation in power: the batteries usually applied have a short lifetime, needing frequent recharging or replacement, which limits the convenience of a wireless operation and increases operation and maintenance costs [2]. Bibliographic

records point to 74% of all the consumed power of a sensor node being directed at the transceiver module [3]. There are three intervention opportunities: to decrease the power consumption of this module; to find a more efficient rate to transmit/receive data, decreasing the time for which the module has to be turned on; and to come up with sustainable energy alternatives that can account for all the power needs of these circuits [4].

Power can be provided to the smart sensor through a connection to the main power grid, with a suitable power transformer, using conventional batteries or harvesting energy from the operating environment. The connection to the main power grid severely hinders the versatility of the devices, namely their ability to be used at different locations. Even though wires are the most reliable, faster and safest way to power anything of electrical nature, the connectors are a weak point, susceptible to moisture and dust and the wiring always limits the portability of the device [4]. Batteries have limited lifetime cycles and cannot be recycled: their internal fuel cannot be replaced and, once spent, the battery has no more use, making them pollutant. Fuel cells, on

* Corresponding author.

E-mail address: pmserra@ubi.pt (P.M.D. Serra).

List of abbreviations	
Π	Reaction quotient
η_{act}	Activation losses
η_{conc}	Concentration losses
η_{ohm}	Ohmic losses
$^{\circ}\text{C}$	Celsius degrees
B, b, B ₁ , b ₁ , C, c, d, D	Polarization curve fitting parameters
BES	Bio-electrochemical system
DC	Direct Current
CH ₃ COONa	Sodium acetate
E _{an}	Anode potential
E _{an} ⁰	Anode potential in standard conditions
E _{cat}	Anode potential
E _{cat} ⁰	Cathode potential in standard conditions
E _{emf}	Electromotive force
I	Absolute current
i ₀	Exchange current density
KCl	Potassium chloride
LP	Low power Sensor
MFC	Microbial Fuel Cell
NaH ₂ PO ₄ (H ₂ O) ₂	Monosodium phosphate (dihydrate)
Na ₂ HPO ₄	Disodium phosphate
NH ₄ Cl	Ammonium chloride
OCV	Open circuit voltage
PCHIP	Piecewise Cubic Hermite Interpolating Polynomial
PMMA	Poly(methyl methacrylate)
PVDF	Polyvinylidene fluoride
R	Universal gas constant
Rx	x can be any number between 1 and 6. This acronym refers to the small volume reactors
RTx	Reactor test x, where x can be any number between 1 and 2
R _{eq}	Equivalent resistance
R _{ohm}	Ohmic resistance contribution on the ohmic losses equation
T	Temperature
ULP	Ultra-low power sensor
V _{mfc}	Microbial fuel cell voltage
V _{ocv}	Open circuit voltage

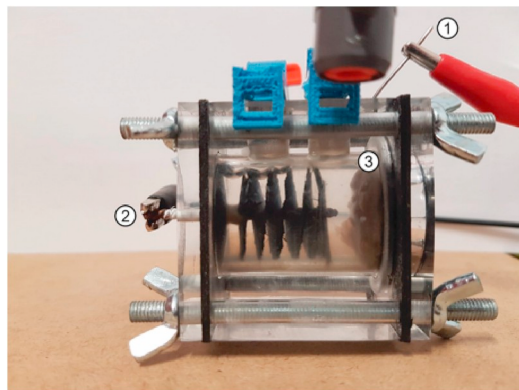
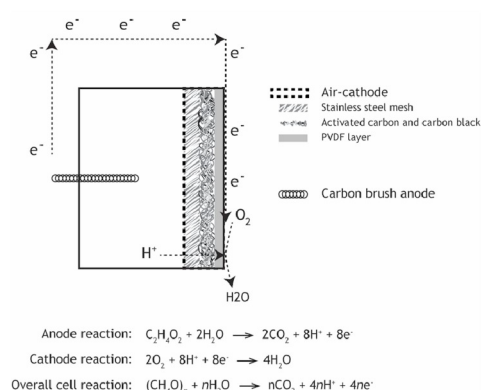
**A****B**

Fig. 1. On the left side, identified by (A): a picture of a 28 mL small volume reactor, where (1) is the titanium wire for cathode connection, (2) is the anode carbon brush and (3) represents the cathode; on the right side, identified by (B) the schematic representation of pictured reactor.

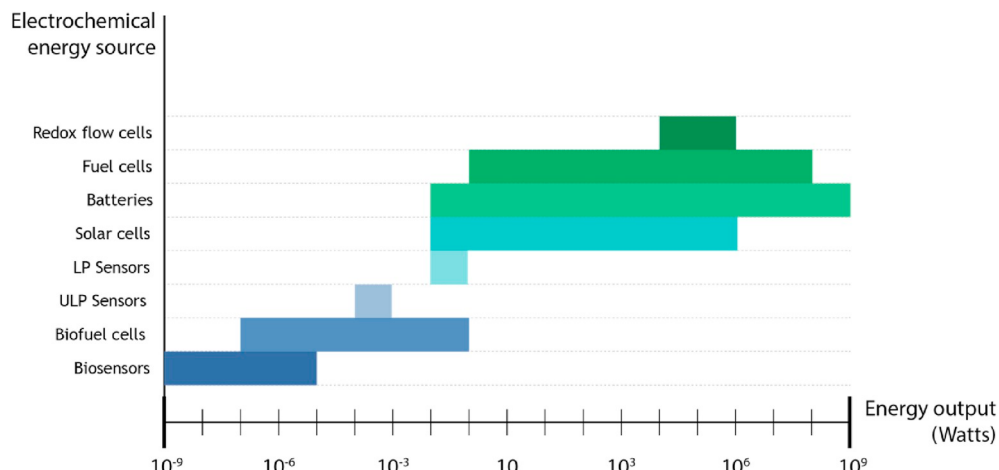


Fig. 2. Energy production levels of electrochemical sources relative to the energy needs of two types of low-power sensor technologies: ultra-low power sensors (ULP Sensors) and low power sensors (LP Sensors).

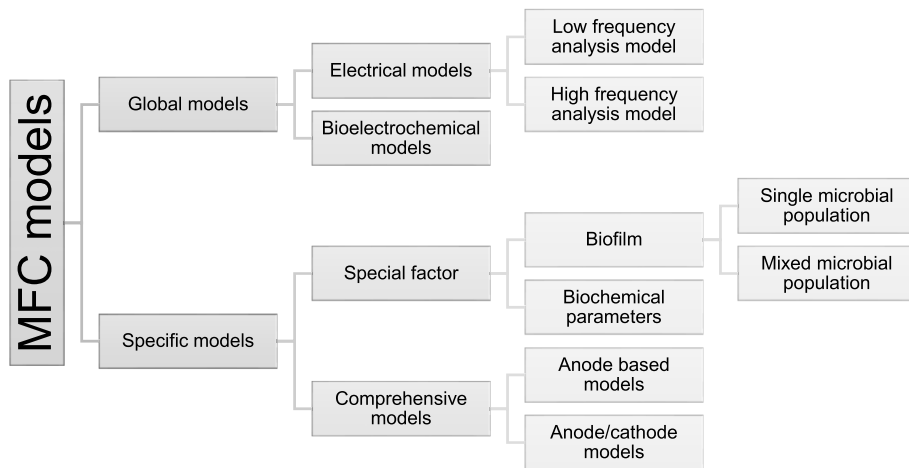


Fig. 3. Possible model categorization for microbial fuel cell studies.

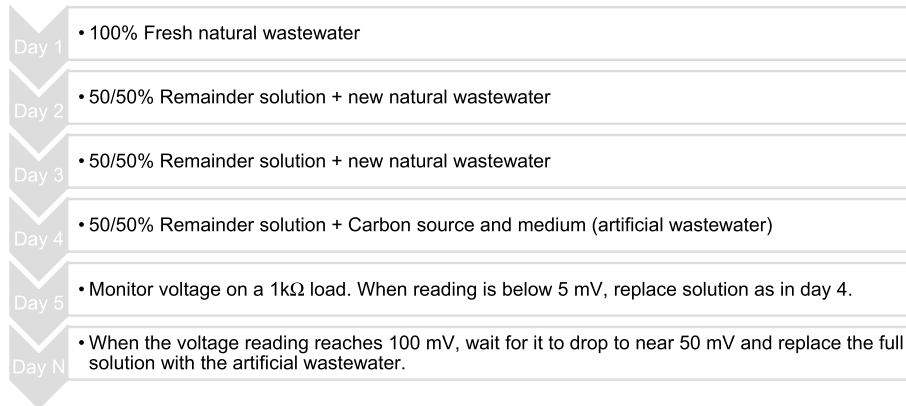


Fig. 4. Inoculation procedure followed for every reactor in the study.

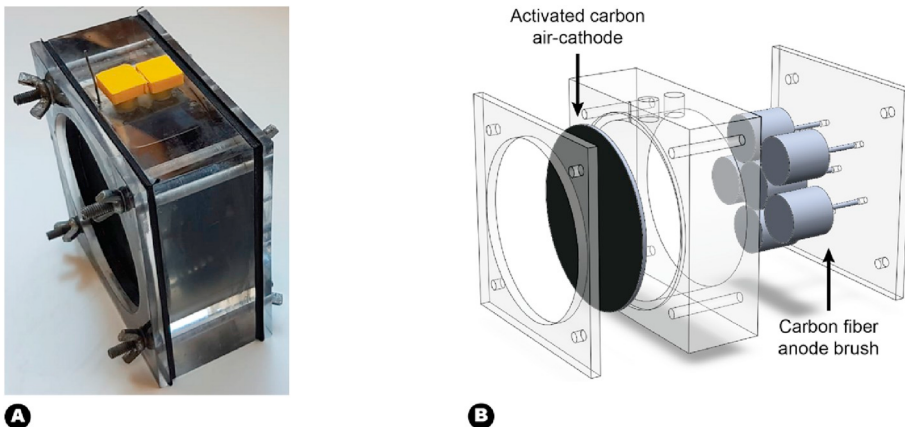


Fig. 5. On the left, identified by (A), a picture of the assembled 250 mL large volume reactor, RT2. On the right, the schematic of the previously mentioned reactor with a blow-out view of the cathode and the 6 carbon brush anodes.

the other hand, can have their fuel replaced, being able to run for a very long time, provided that no other element is damaged. They can also be pollutant if their electrolyte is inorganic and cannot be recycled. The solution to this challenge resides on energy harvesting, also called power harvesting or energy scavenging: in such a scenario, the energy need is met by harvesting readily available and renewable energy at the site, using it in a well-timed fashion. For low power needs, energy can be harvested from electromagnetic sources (ambient radio frequency, RF),

electromechanical transducers (vibration, piezoelectric) and from temperature, pressure or salinity gradients. Harvesting energy from biological sources is a new challenge being explored: though having a limited bio-electro-chemical knowledge, we are at the point where we can use that insight to recover/redirect "biological" power to our benefit. For most environmental sensors, the measurement requirements can be addressed with power in the range of milliwatts [5]. Microbial Fuel Cells (MFCs) are a type of bio-electrochemical system (BES) where

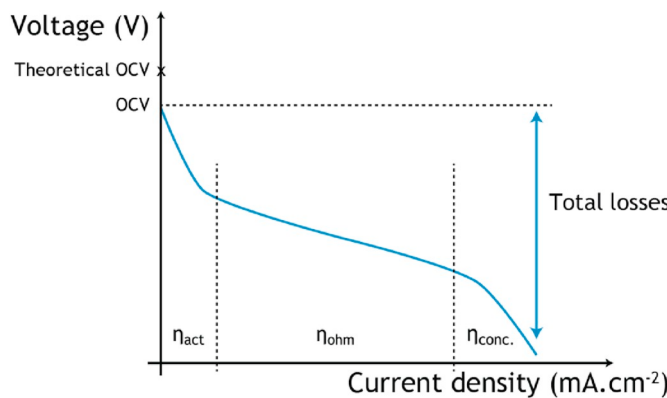


Fig. 6. An example of a polarization curve.

energy is retrieved from bacteria feeding of an organic substrate in anaerobic conditions. A review of the literature published since 1994 on microbial and enzymatic biofuel cells is provided in Ref. [6]. The increasing interest of electroactive microorganisms applications by means of bioelectrochemical systems is discussed in Ref. [7] presenting the performance of different types of MFCs. The detailed operation of MFC and the conversion of organic wastes into energy is documented in Refs. [8,9]. Additionally, structural information about MFCs' materials and several examples of application can be found in Ref. [10]. A standard design of a single chamber air-cathode MFC is presented in Fig. 1, along with the equations describing the involved reactions for an acetate-based substrate.

MFCs can be used wherever a liquid organic source for carbon is available, provided the source is not toxic and the environment adequate for the bacteria. As such, MFCs can be applied to wastewater treatment plants, either for industrial, sewage or agriculture wastewater, being useful for powering ultra-low power (ULP) and low power (LP) sensors, as shown in Fig. 2.

In order to accurately predict if the power profile of an MFC can fit the energy needs of the aforementioned sensors, both in magnitude and

in time, an electrical model of the MFC is paramount. The maximum voltage level that can be produced by any fuel cell corresponds to its electromotive force, or E_{emf} , derived with the Nernst equation:

$$E_{emf} = E_{cat} - E_{an} \quad (1)$$

where E_{cat} represents the cathode potential and E_{an} the anode potential. These potentials can be determined if the reaction equation, the concentration of each oxidizing and reducing agent and the specific temperature is known:

$$E_{cat} = E_{cat}^0 - \frac{RT}{nF} \ln(\prod) \quad (2)$$

and

$$E_{an} = E_{an}^0 - \frac{RT}{nF} \ln(\prod) \quad (3)$$

where, E_{cat}^0 and E_{an}^0 represent the electrode potential in standard conditions (298.15 K, 1 bar pressure, 1 M for all species), R corresponds to the universal gas constant, T is the temperature in Kelvin and \prod is the reaction quotient. The reaction quotient is a chemical measure of the relative amounts of the reactants and the products according to time.

For a neutral pH of 7, acetate oxidation at the anode, and oxygen as the electron acceptor at the cathode, the theoretical E_{emf} is of 1.1 V. The E_{emf} , however, cannot be achieved since fuel cells have inherent internal energy losses related with, for instance, the unbalanced proportion between reactants and products or reversibility of the oxidation-reduction reaction, and its internal resistance, a result from the materials and geometries chosen for the cell. These losses are derived from the material characteristics, the bacterial profile and the substrate composition. Contrary to what happens in other fuel cells without living species, the microbes on MFCs have numerous metabolic options for energy production. This has a major negative impact on the predictability of MFCs, conditioning the development of a unified model for MFC behavior. Therefore, several models are available, developed to different ends [11–14]. A unified proposal for a classification model is suggested by the authors in Fig. 3.

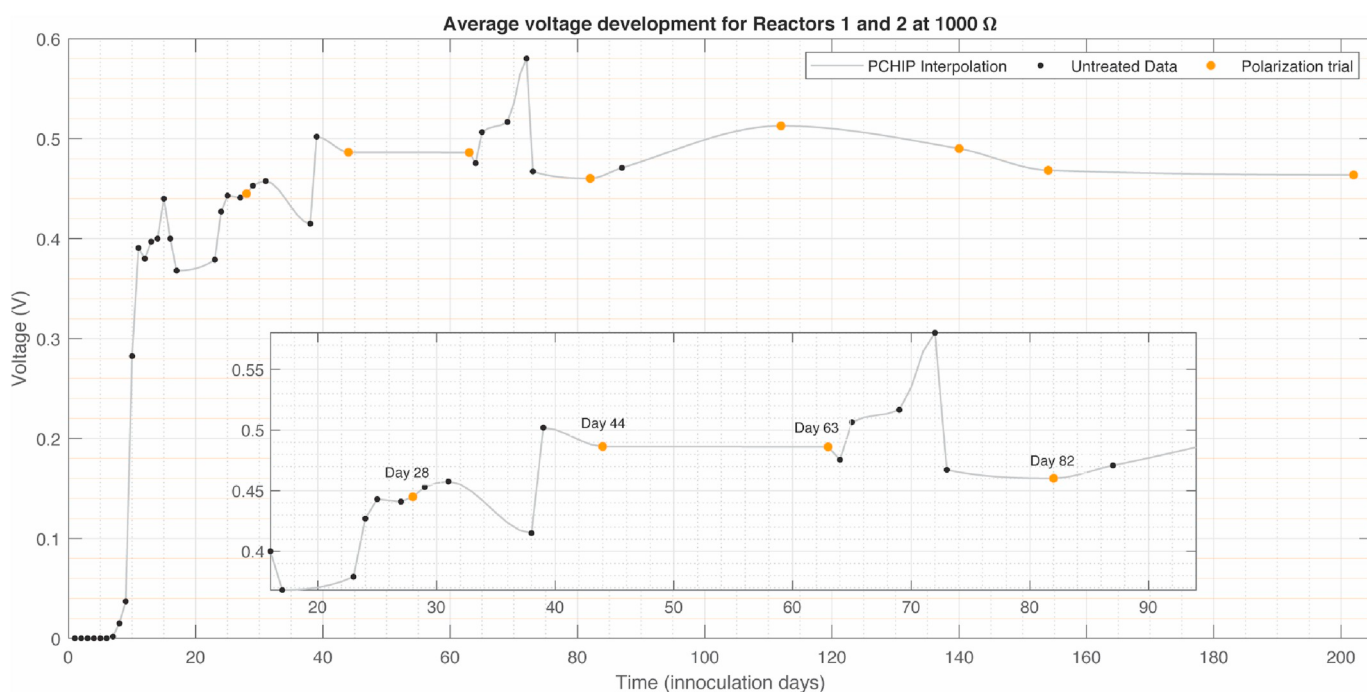


Fig. 7. Average voltage development for 1000Ω load. The cross marks pinpoint the polarization runs and black dots the averaged voltage levels for R1 and R2. The interpolation method applied was Piecewise Cubic Hermite Interpolating Polynomial (PCHIP).

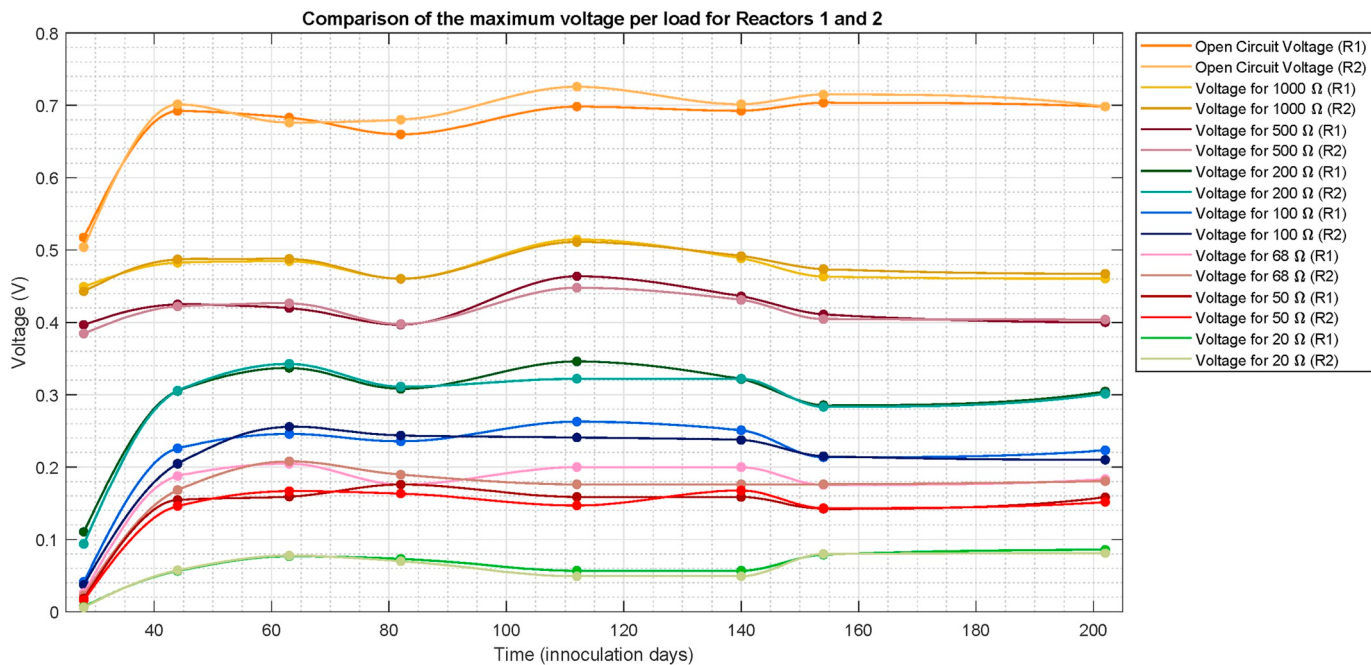


Fig. 8. Voltage development for different loads in reactor 1 and 2 for 202 days. Only data from R1 and R2 is pictured because they had significantly more inoculation time than the other reactors on the set.

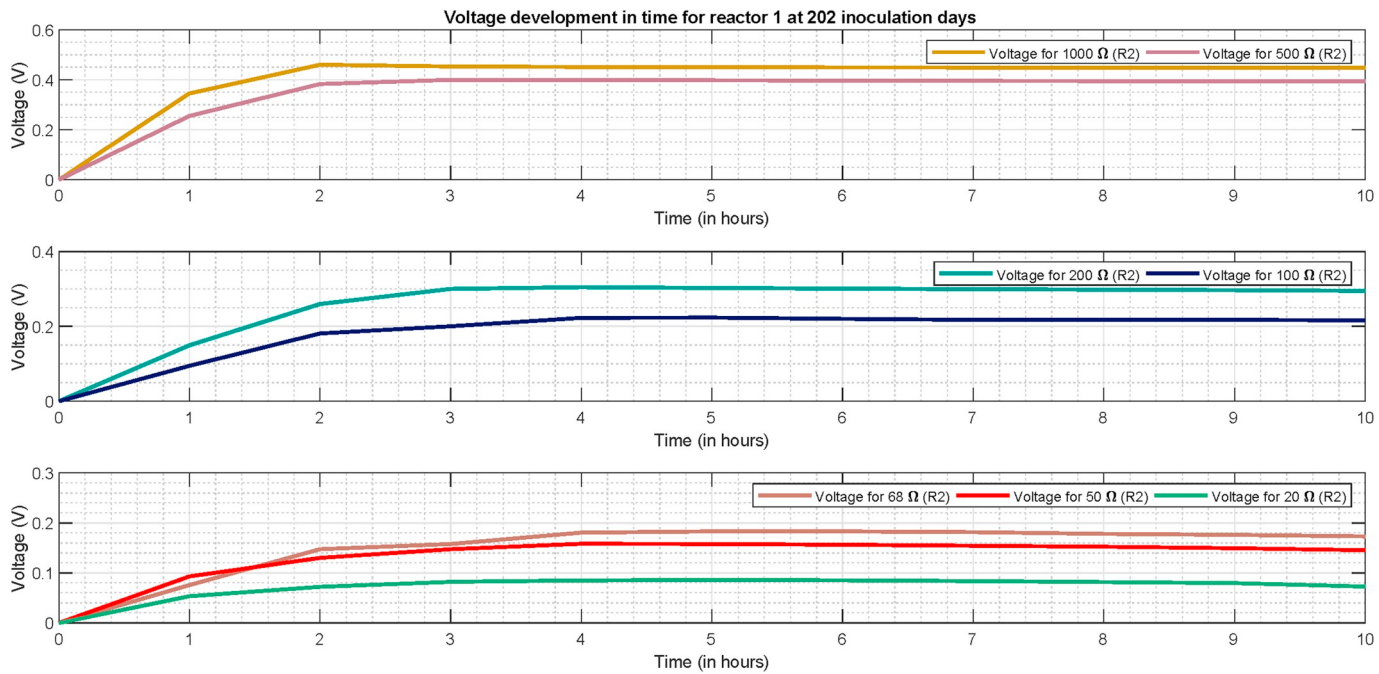


Fig. 9. Voltage development for different external loads at 202 inoculation days of R1.

Each model describes an MFC from a different perspective and should be applied carefully and according to its intended final use. For instance, an anode-based model should not be used to describe the MFC behavior regarding the biofilm growth and substrate consumption, since the latter is better characterized by a biochemical parameter model.

Considering that the bacteria age and diversity on the anode biofilm, the substrate, the anode, the cathode and the reactor volume all differently impact a Microbial Fuel Cell's electrical behavior, this article reports on the study of a particular type MFC air-cathode reactor, estimating its internal power losses and identifying their contribution on the overall polarization curve. Other studies have also been developed

with similar reactors, allowing for some data comparison [15]. In spite of all the variability in play, a discussion of the results will show that the polarization curve typology is adequate for the electrical behavior description and that, additionally, the steady state response can be even be further simplified. The use of such an equation will allow for the development of an electrical model to help dimension a boost converter for this technology and its use to activate low power self-sustained sensors in remote or difficult access locations.

The following discussion is focused on data analysis from polarization trials applied to microbial fuel cells. Section 2 exposes the data collection, details on the reactors used for the study, and the proposed

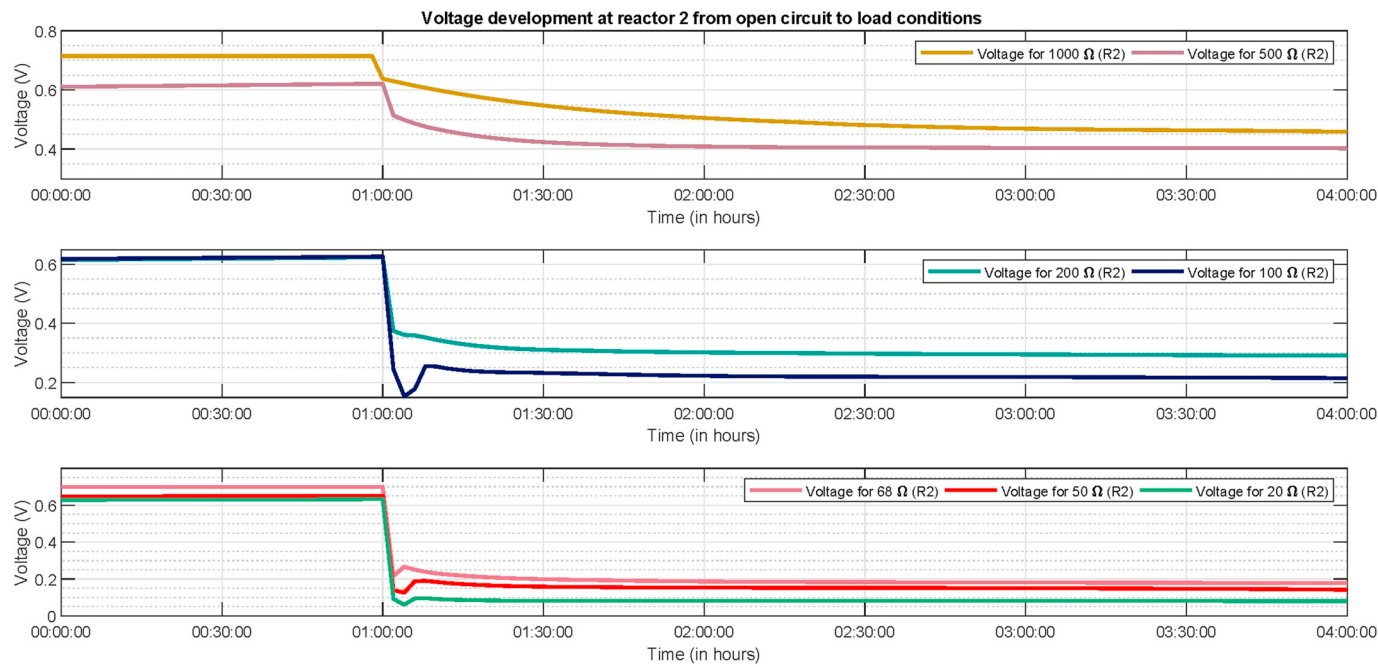


Fig. 10. Voltage profile from open circuit to load transition.

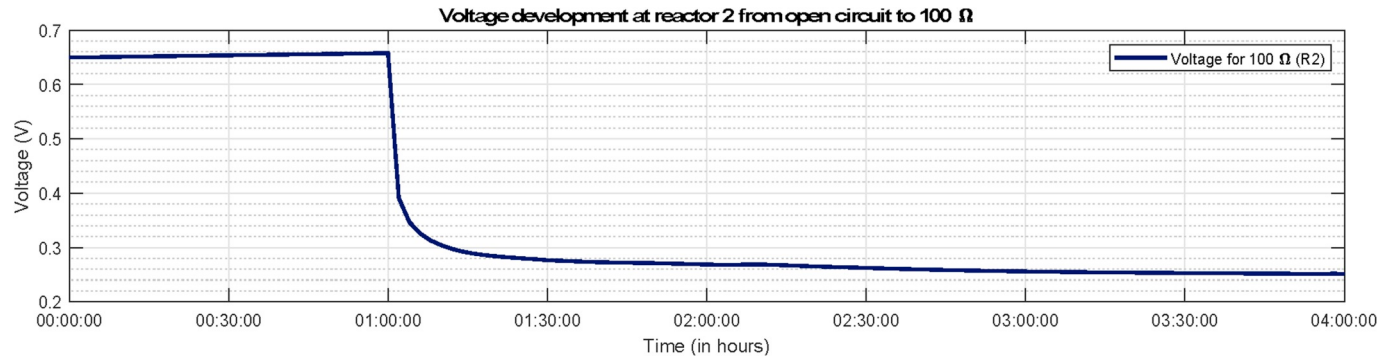


Fig. 11. Voltage profile from open circuit to $100\ \Omega$ transition.

procedure for obtaining the polarization equation. Section 3, results and discussion, begins by relating power development with the inoculation time. The analysis continues by intertwining time and external loads with power. A steady-state analysis ensues and the equation for estimating the reactor's internal resistance is then presented. The method for obtaining the polarization equation is further explored by applying it to a similar reactor on a different study and to a large volume reactor with the same geometry and materials. From this equation, an electrical circuit model is proposed as a way to conduct simulations for optimizing the development of a power conditioning stage.

2. Materials and methods

Experimental data points were collected by using single-chamber air-cathode reactors, based on the work by Ref. [16], with a 28 mL cylindrical inner chamber. The reactors were made out of Poly(methyl methacrylate) (PMMA) and both the electrodes were carbon based: the anode a carbon fiber brush and the cathode a stainless-steel flat disk covered by a Polyvinylidene fluoride (PVDF) mixture of carbon black and activated carbon. Details on the electrodes and reactor geometry can be found in Ref. [17]. The anode carbon brush, prior to its application, was subjected to a 30 min $450\ ^\circ\text{C}$ temperature treatment.

A group of 6 reactors (Rx) was tested. These reactors will be

identified by R1 through R6, accordingly. After being assembled and tested for water tightness, the reactors were inoculated according to Fig. 4.

The natural wastewater was collected from a wastewater treatment plant in the city of Covilhã (Portugal) and the electrodes were connected through a $1\ \text{k}\Omega$ load during all the inoculation procedure. Voltage was monitored at every day of the inoculation, although only registered at the polarization runs. After day 4, the solution was replaced, with the quantities as in the fourth day, when the voltage reading was below 5 mV. After voltage readings reached 100 mV and dropped to near 50 mV, the complete solution was replaced by the artificial wastewater of carbon source and medium, which composition follows [18] and the below proportions:

- CH_3COONa – 1 g/L;
- $\text{NaH}_2\text{PO}_4(\text{H}_2\text{O})_2$ – 2.772 g/L;
- Na_2HPO_4 – 4.58 g/L;
- NH_4Cl – 0.31 g/L;
- KCl – 0.13 g/L

Of the six reactors, and until the 9th of September 2018, R1 and R2 where inoculated for 7 months, about 200 days, where 8 polarization runs were made. The other four reactors (R3, R4, R5 and R6) where

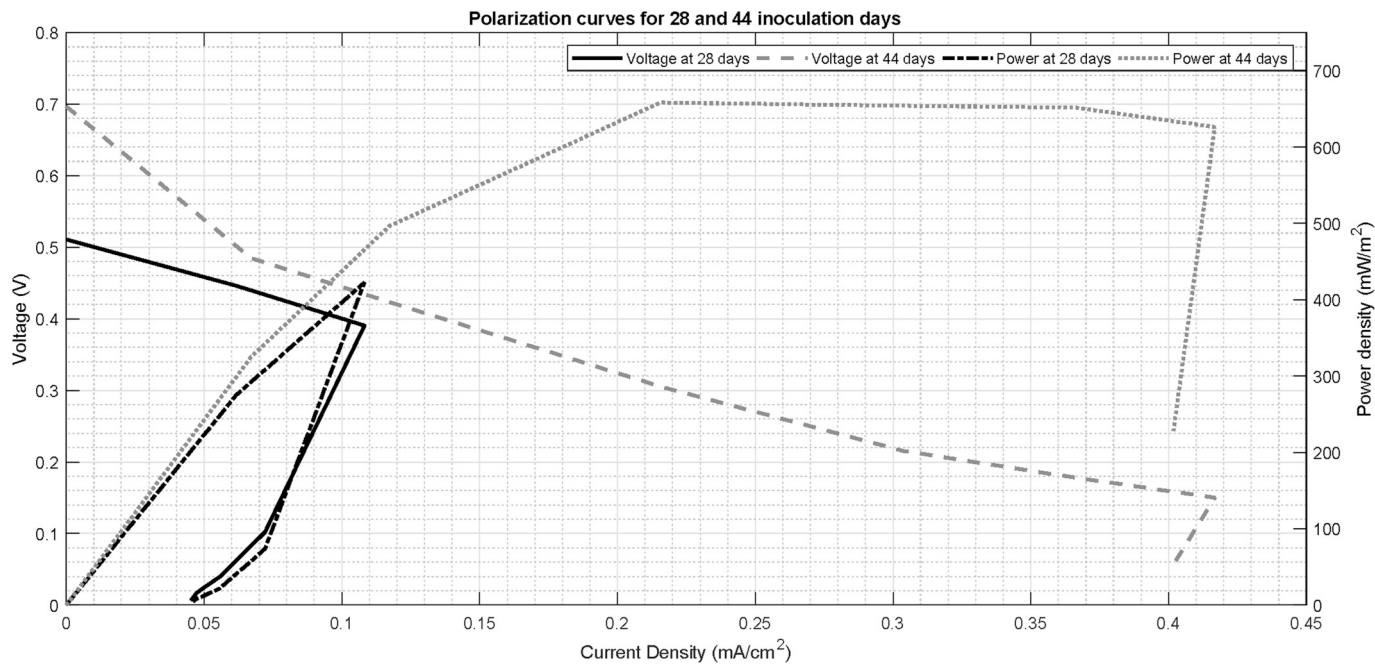


Fig. 12. Polarization curves built from averaged voltage values per external load at 28 and 44 inoculation days.

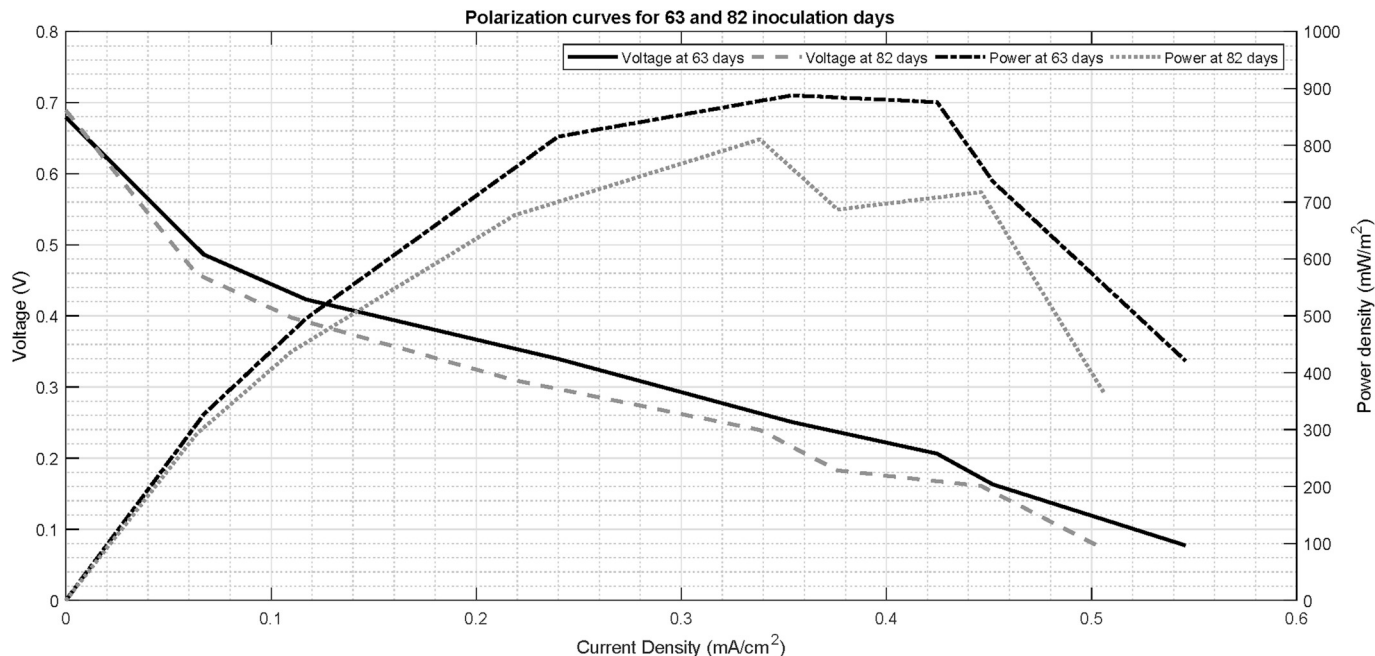


Fig. 13. Polarization curves built from averaged voltage values per external load at 63 and 82 inoculation days.

inoculated for 5 months, about 150 days, with 2 polarization runs. The second batch of reactors was subjected to varying external loads – from $1\text{ k}\Omega$ to $20\text{ }\Omega$ – before conducting a monitored polarization run: after voltage readings at $1\text{ k}\Omega$ were constant, the load was lowered at every artificial wastewater change. This procedure was repeated until voltage readings at $20\text{ }\Omega$ equaled or surpassed the readings found, at the same load, for the reactors from the first batch (reactors 1 and 2).

The polarization data reported in Ref. [15] was retrieved and used to further proof the proposed method applicability, due to the similarity between electrodes, reactor and the substrate of that and this work. This reactor will be identified by RT1, meaning reactor test 1.

The algorithm robustness was also tried against the polarization data

of a large volume reactor. This reactor will be referenced by RT2. Although with 9 times the volume of the Rx reactors (approximately 250 mL) – with 6 parallel connected anode carbon brushes and a cathode with 9 times the area of the one in the small reactors (built with the same phase inversion method) – the reactor, shown in Fig. 5, respected the same geometry and electrode spacing.

The polarization curves were collected by applying the multi-cycle method [17,19], with a set of 7 resistances varying from $1000\text{ }\Omega$ to $20\text{ }\Omega$. The resistance change was applied when changing the artificial wastewater, which guaranteed no wastewater batch was subjected to different loads. Voltage was registered every 2 min by a mbed LPC1768 for at least 4 h. Data was processed in MATLAB 2018 and GraphPad

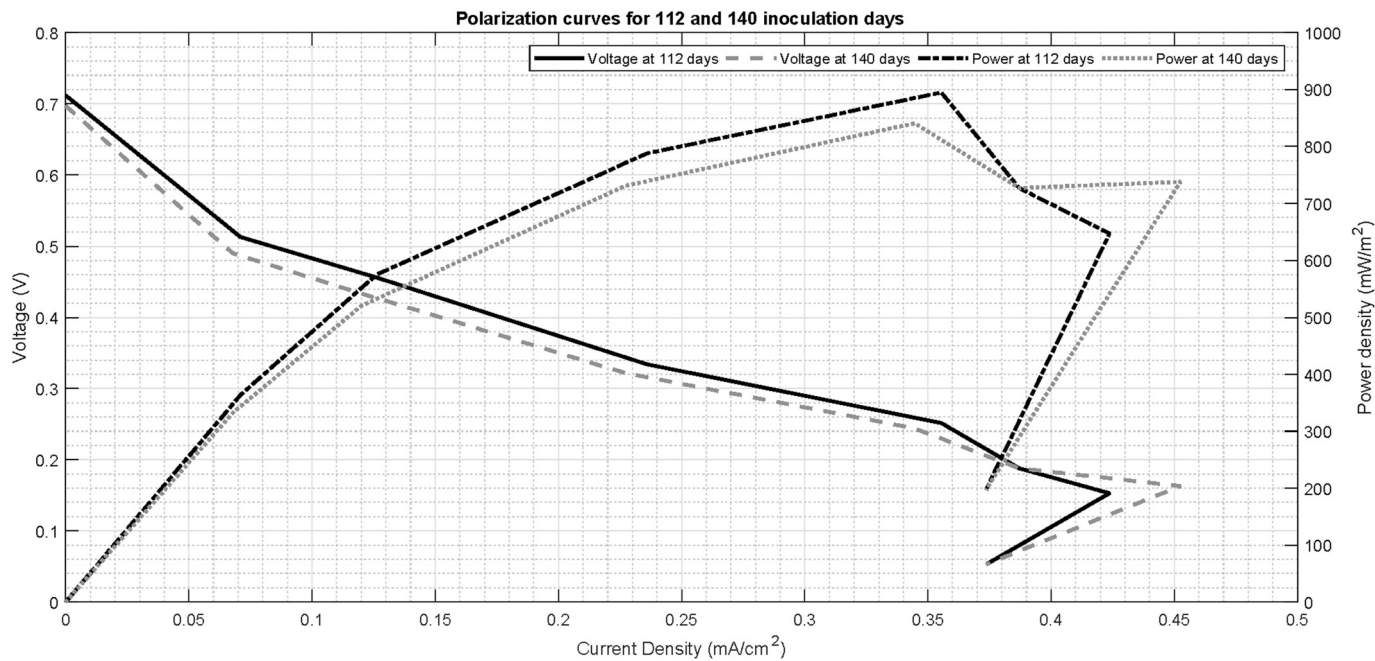


Fig. 14. Polarization curves built from averaged voltage values per external load at 63 and 82 inoculation days.

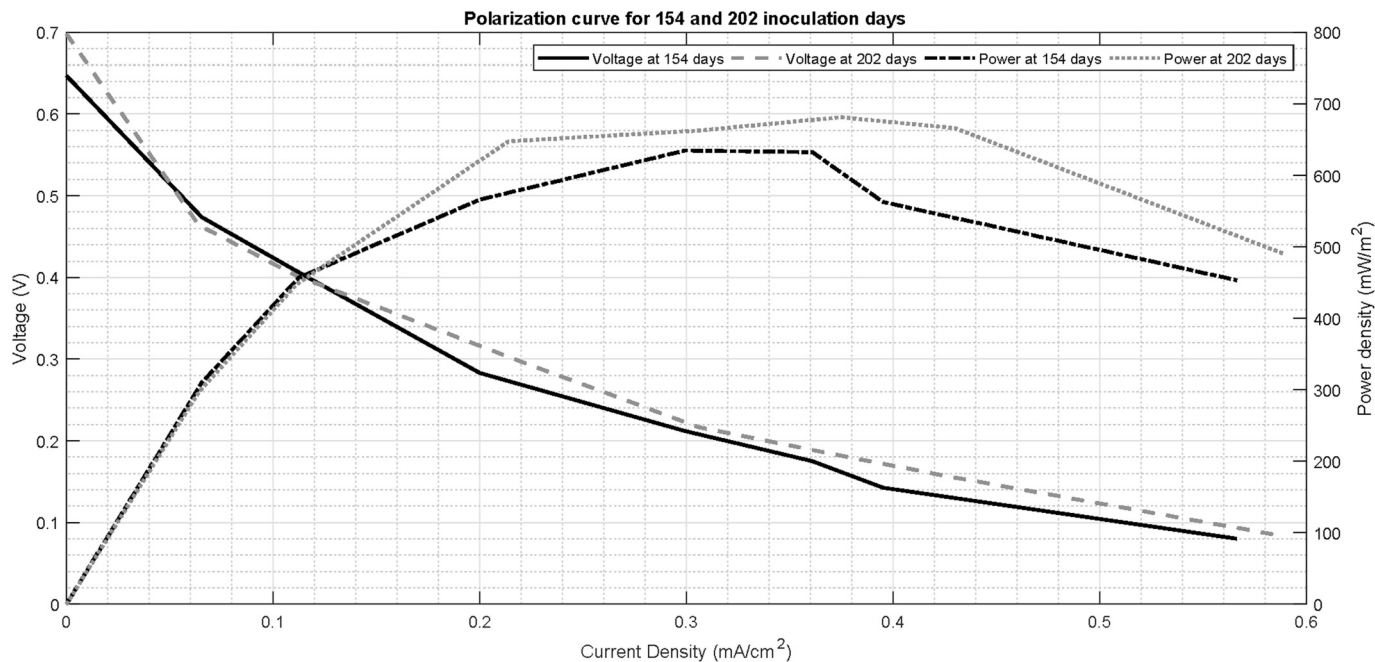


Fig. 15. Polarization curves built from averaged voltage values per external load at 154 and 202 inoculation days.

Prism 7. To determine the voltage achieved at each resistance load and to constrain the influence of artefacts and non-sustainable values, each reported value results from averaging the voltages for 1 h. The maximum per load is than the maximum value found in that trial. The analysis on GraphPad Prism 7 consisted on importing the polarization data and applying two fits to the voltage-current curve: firstly a linear fit for estimating the internal resistance of the reactor, a parameter which rounds up all its direct and indirect contributions; secondly, a non-linear least squares fit to estimate the parameters best describing the data. The linear regression is applied to a set of 3 values: one voltage-current pair under, one equal and one over the voltage-current pair corresponding to the maximum power. This approximation will allow estimating the

internal resistance of the reactor – the slope on the linearization equation – according to the maximum power point theorem, where the maximum power is achieved when the internal and external load are equal. The non-linear regression, used for determining the full equation describing the polarization curve, outputs estimates for all the variables by setting the OCV value to the experimentally determined, the ohmic resistance to a value smaller than the internal resistance estimate from the linear regression, and all the other parameters to be positive.

When studying fuel cells, polarization studies are very useful to identify power losses. After identified, they can be corrected, and new polarization studies can clarify if the solutions applied led to a power increase. A polarization curve retrieved from varying the external load

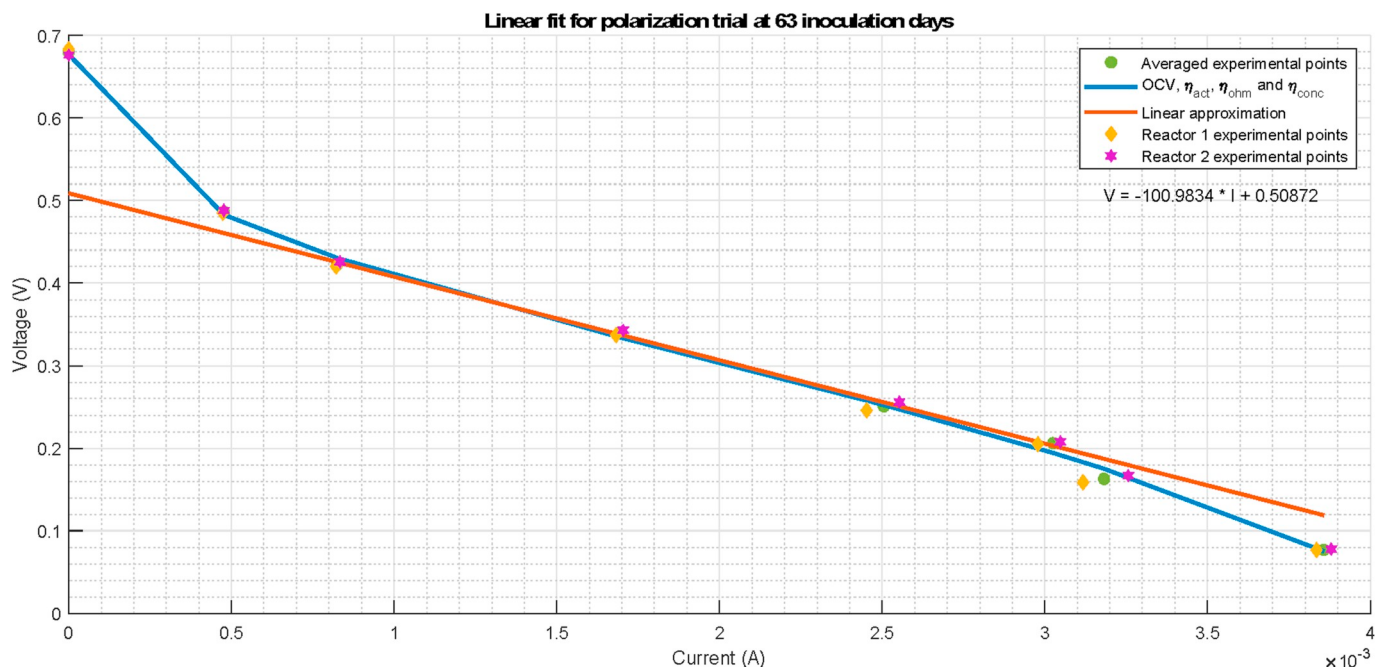


Fig. 16. Linear fit for loads between 200 and 68 Ω at 63 inoculation days. The plot also shows the relationship between the averaged experimental points, the actual points for each reactor and their proximity to the steady-state equation.

Table 1

Parameter estimation through GraphPad Prism 7 for non-linear regression and linear regression for internal resistance.

Parameter	Values for non-linear regression	Value for linear regression
A	Fixed at 679.5×10^{-3} V	
B	636.5×10^{-4}	
B ₁	3.628×10^{-5}	
R	50.51 Ω	$\approx 100 \Omega$
C	2.671×10^{-3}	
D	967.4	

and measuring the output voltage has an outline similar to that on Fig. 6.

In this curve, three regions can be identified. Each of them is associated with an overpotential. Charge overpotentials (η_{act}), or activation losses, happen at low currents and start from the open circuit voltage (OCV). The theoretical OCV refers to the E_{emf} . Charge overpotentials result from the energy needed for reactions to happen at the electrode's surface. The linear region of the graph corresponds to ohmic losses (η_{ohm}) due to ionic resistances in the MFC. The last region corresponds to the mass transport or concentration losses (η_{conc}): at high currents, the concentrations of reactants and/or products get unbalanced and their flux becomes sluggish. Both the activation and the mass transport losses exhibit a non-linear behavior. The research provided in Refs. [20,21] discusses electrochemical/electroanalytical techniques employed in the experimental study of MFC presenting and discussing these techniques. In the example provided in Ref. [22] a power management system is proposed with the main goal of at first store the energy provided by the MFC and next power the wireless device. Details about experimental methods to study and evaluate the performance of MFCs are presented in Refs. [23–25].

The relative magnitude of each of the losses gives relevance towards the optimizations that can be implemented for the MFC to peak its power production capabilities.

3. Results and discussion

Voltage development was closely followed during reactor inoculation, for R1 and R2. Fig. 7 shows the averaged values for 202 inoculation days.

The unsteady development of the voltage profile in the first 15 days represents some issues with the reactors' watertightness. Still, the bacterial biofilm developed successfully, and the polarization runs started after 28 days of inoculation. The first few days of inoculation do not present meaningful voltage values since the bacterial population is not using anaerobic respiration for their metabolism, which means the electrodes aren't being used. The first step to force this metabolic choice is to limit the reactor's oxygen exposure. This procedure will help select bacteria exhibiting exoelectrogenic behavior, but with associated voltage decrease. At the fourth day, and by adding the artificial wastewater rich in sodium acetate, the selected bacteria begin to grow and multiply, which, in turn, increases the measured voltage levels.

Data from R1 and R2 shows that, irrespective of the reactor, voltage profiles for the same loads exhibit the same behavior and very close final values, as showed in Fig. 8. Having had the same wastewater and time for inoculation, it is safe to assume that the bacterial community composition must be very close, meaning that polarization trials for similar reactors with the same inoculation time return values with little discrepancy. Value fluctuations can be attributed to changes in the electrode's characteristics, namely cathode biofouling.

The voltage development for an MFC is neither linear with load nor with time, as can be seen by Fig. 9. Data here represented was gathered by starting voltage monitoring as soon as a reactor was refilled with a new wastewater batch.

The voltage development for an MFC exhibits properties that change according to the load value. The steady state voltage value is achieved after a specific time, which is dependent on the load and the biofilm complexity. To determine the real influence of the load on the transient response, a trial was conducted where voltage was monitored on the transition from open circuit to a load, applying the multi-cycle method, as showed in Fig. 10.

Such trial showed that 1 h after the load application, the voltage value stabilizes to around 90% of the final value, irrespective of the load

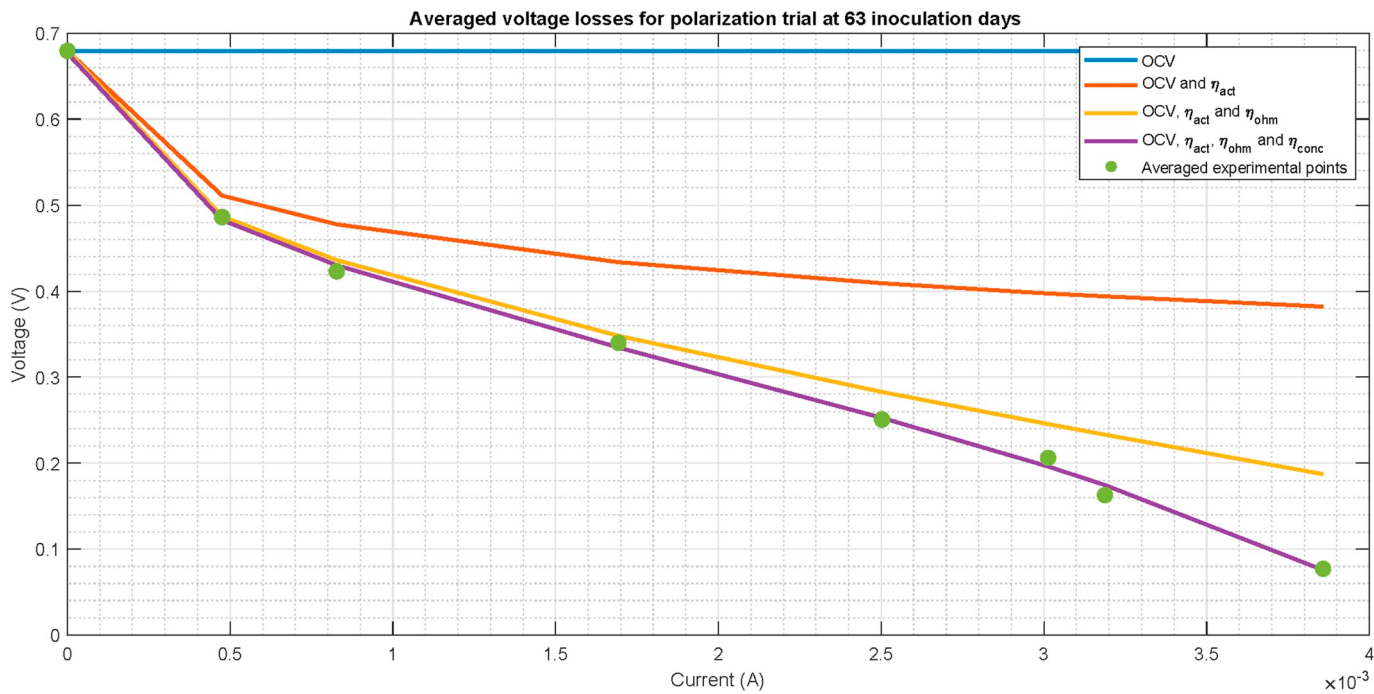


Fig. 17. Polarization curve built from averaged voltage and current values per external load at 63 inoculation days.

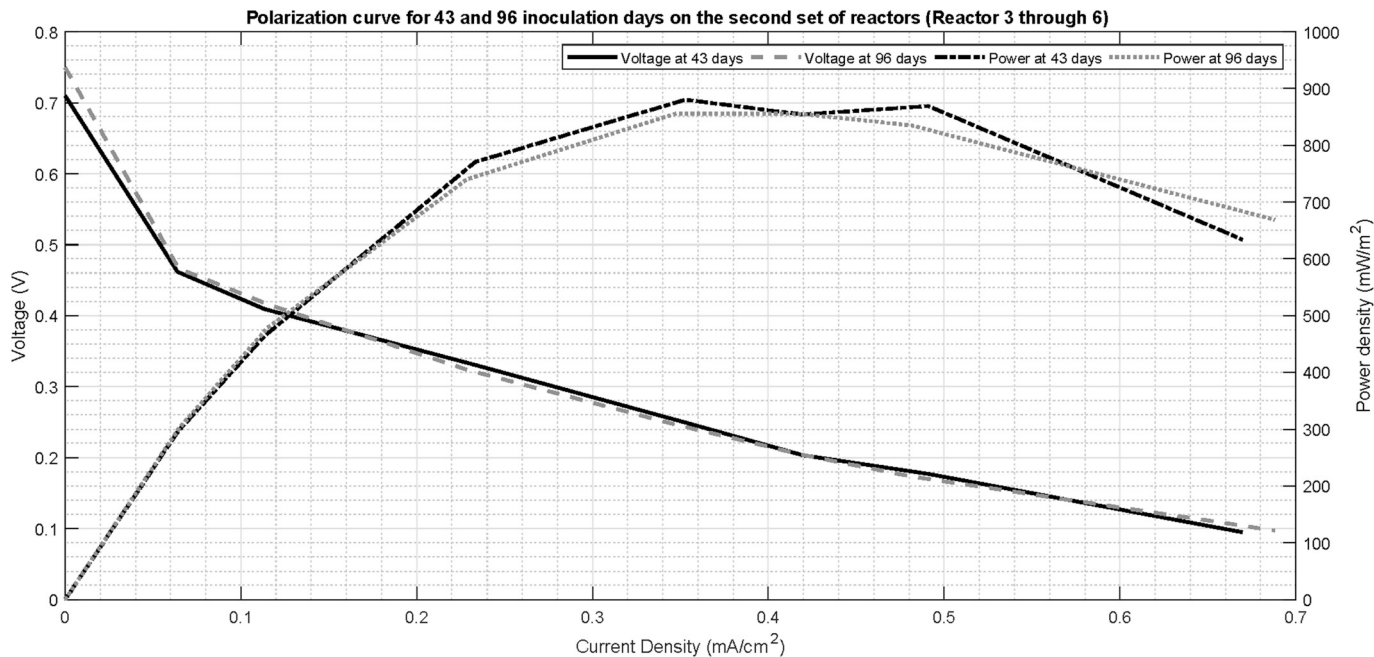


Fig. 18. Polarization curves built from averaged voltage values per external load at 43 and 96 inoculation days for reactors 3 through 6.

magnitude. It is noticeable, however, that loads of 1000 and 500 Ω need more time for voltage stabilization than loads under 200 Ω .

By knowing the response presents little to none oscillations after 1 h, polarization trials can be conducted reliably and for shorter times.

The elbow behavior on the open-circuit load transition for resistances under 200 Ω in Fig. 10 does not follow the behavior for other loads. It is not clear if this performance was specifically related with the biofilm characteristics or, rather, if it was a consequence of repeatedly having the reactors in open-circuit for around 3 h before applying the load. As such, a trial of open-circuit to load transition for 100 Ω was repeated, after subjecting the R2 to 100 Ω during 2 consecutive

wastewater batches. The results are presented in Fig. 11.

By analysis of the data on Fig. 11, it can be concluded that successive open-circuit to load trials have a negative impact on the maximum voltage per load. Furthermore, it is also clear that the elbow behavior does not accurately describe the voltage transition at load connection. Although relevant for determining a dynamic electrical model for MFCs, the specific details on the transient behavior of a Microbial Fuel Cell are out of the scope of this current work.

The biofilm maturation stage can be determined by running polarization trials on the reactors. As previously discussed, several trials were conducted. To clearly summarize these results, data was grouped by

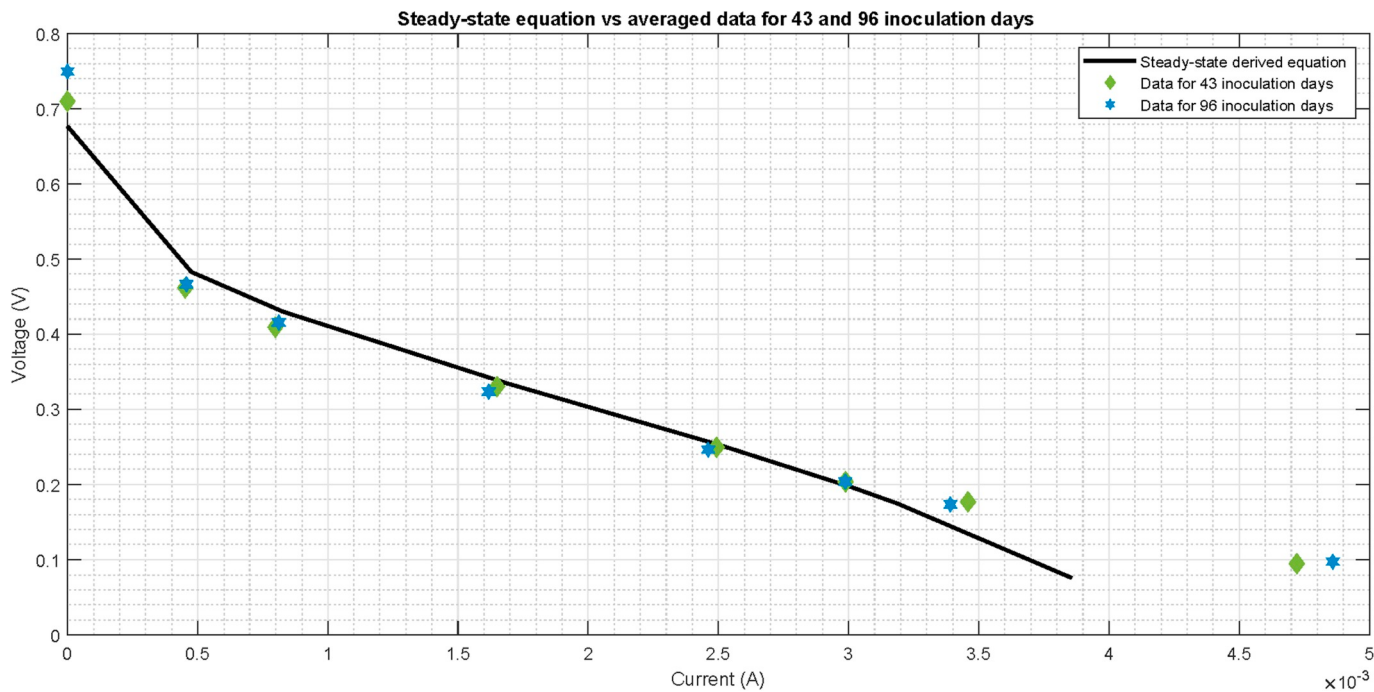


Fig. 19. Polarization curves built from averaged voltage values per external load at 43 and 96 inoculation days for reactors 3 through 6.

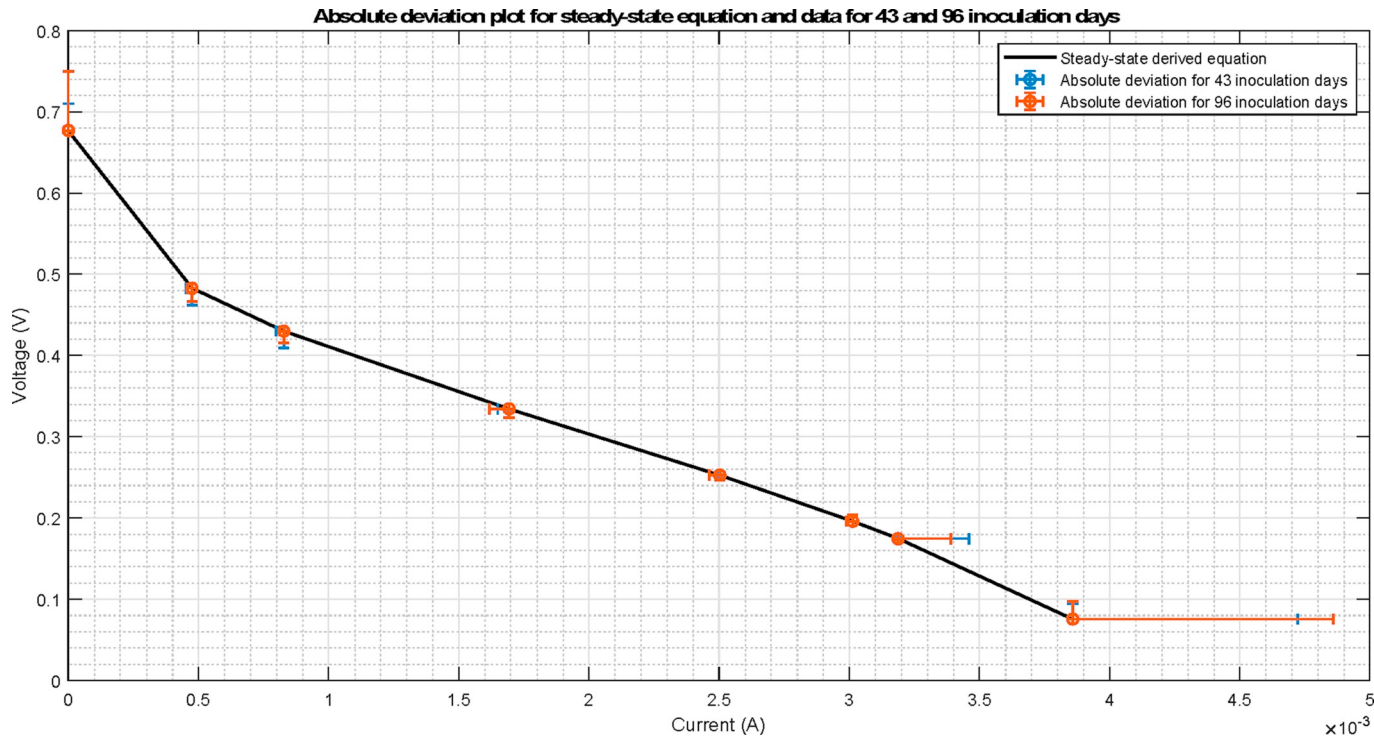


Fig. 20. Absolute deviation of the experimental data and steady state equation for polarization trials at 43 and 96 inoculation days for reactors 3 through 6.

averaging the voltage values for R1 and R2 for the same external loads. To allow inter and intra study comparison, current and power are reported in reference to the cathode area (7.07 cm^2). Data was further clustered for plotting purposes by grouping polarization trials by sets of inoculation days, as presented in Figs. 12–15.

Data on Fig. 12 depicts a phenomenon called power overshoot. Power overshoot is the phenomenon found at high current densities after the maximum power point, where the cell's voltage and current

drops to lower values, producing lower power values than achieved before. Simply put, a voltage drop results in a current drop and leads to a bending on the polarization curve [19,26]. As referred in Ref. [27], this phenomenon is common in reactors acclimated to high external resistances and tends to disappear when the anodic biofilm matures and develops adequate redox enzymes for high current densities. Even so, the reactors averaged a maximum power of 658 mW/m^2 (0.465 mW at approximately 305 mV and 200Ω) at 44 inoculation days.

Table 2

Relative error, in percentage, between the steady state curve and the averaged data from trials at 43 and 96 inoculation days.

Load (Ω)	Relative deviation from Steady State equation			
	43 inoculation days		96 inoculation days	
	Voltage deviation (%)	Current deviation (%)	Voltage deviation (%)	Current deviation (%)
OCV	4.30	0	9.34	0
1000	-4.59	-5.11	-3.50	-4.08
500	-5.05	-3.71	-3.43	-1.98
200	-1.20	-2.63	-3.26	-4.66
100	-1.20	-0.38	-2.60	-1.70
68	3.76	-0.83	3.80	-0.86
50	1.39	7.85	-0.60	6.02
20	20.23	18.29	22.35	20.62

The plots on Fig. 13 are sharper representations of an adequate polarization curve. The losses are more easily identified in each of the different slopes of the IV curve. A maximum power of about 887 mW/m² (0.627 mW at approximately 250 mV and 100 Ω) was achieved at 63 inoculation days. The polarization trial conducted at 82 days shows signs of decreased reactor performance. In between polarization trials, the reactors were kept with fresh feedstock and the electrodes connected through an external resistance. Since the external resistance was the same, around 1 k Ω , the biofilm's ability to answer to low external resistances with high currents became hindered (the high current redox enzymes became less expressed).

The analysis of the plots on Fig. 14 is a further proof of the reactor's performance drop. A power overshoot is again found, with a harsher drop on the plot for 112 days. This performance limitation is already being addressed at the trial on 140 inoculation days, since the external load between trials was lowered to 500 Ω . This is why a second peak is found around 0.45 mA/cm²: the biofilm is already more successful in answering to a higher current request, although not capable of a complete follow-up and doubling back at around 20 Ω . A maximum power of approximately 895 mW/m² (0.632 mW at approximately 250 mV and 100 Ω) was achieved at 112 inoculation days.

The analysis of the plots on Fig. 15 shows that the biofilm was successfully re-adapted to higher current densities – by varying loads in the complete polarization range – since no power overshoot is found.

However, the maximum power dropped, reaching values close to 680 mW/m² (0.481 mW at approximately 180 mV and 68 Ω) at 202 inoculation days. This decreased power density is due to biofilm build-up on the cathode: although anaerobic conditions are constantly being applied to the reactors, the cathode surface is highly aerobic, due to the needed cathode oxygen permeability. As such, specific bacteria can adhere to the cathode and use oxygen directly, bypassing the anode usefulness. This phenomenon has a slow onset, but once started it can only be stopped by appropriate cleaning of the cathode [28] and the reactor or, as a last resource, by applying a new cathode.

Of all the polarization trials run, and according to the previous discussion, data from the trials at 63 inoculation days is better suited for determining a general equation for reactors with this specific set of characteristics and artificial wastewater composition.

3.1. Deriving a steady-state equation for characterizing polarization curves in MFC

Considering only the response in steady-state, an equation can be derived from all the electrochemical losses. The activation losses (η_{act}) can be modeled from the Tafel equation:

$$\eta_{act} = b \times \ln(i_c / i_0) \quad (4)$$

where b is related with the cell's characteristics: the higher the value, the slower the reactions; i_c represents the MFC's current density and i_0 the exchange current density. The exchange current density characterizes the catalytic ability of the electrode's surface: higher i_0 values are related with faster reactions. In MFC's, current densities are usually expressed in mA/cm². This equation is only applicable when $i_c > i_0$, since there are no circumstances where there are no activation losses ($i_c = i_0$) or where they add up to the outputted voltage ($i_c < i_0$). As previously mentioned, the analysis will be applied to the steady-state behavior, which means that the variables i_c and i_0 have a constant relationship. As such:

$$\eta_{act} = b \times \ln(i_c / i_0) = b \times \ln(i) \quad (5)$$

This approximation is valid for currents over 1 mA/cm², since $\ln(1) = 0$. For $i < 1$ mA/cm²:

$$\eta_{act} = b \times \ln(i) = b \times \ln\left(\frac{i}{i_1} + 1\right) \quad (6)$$

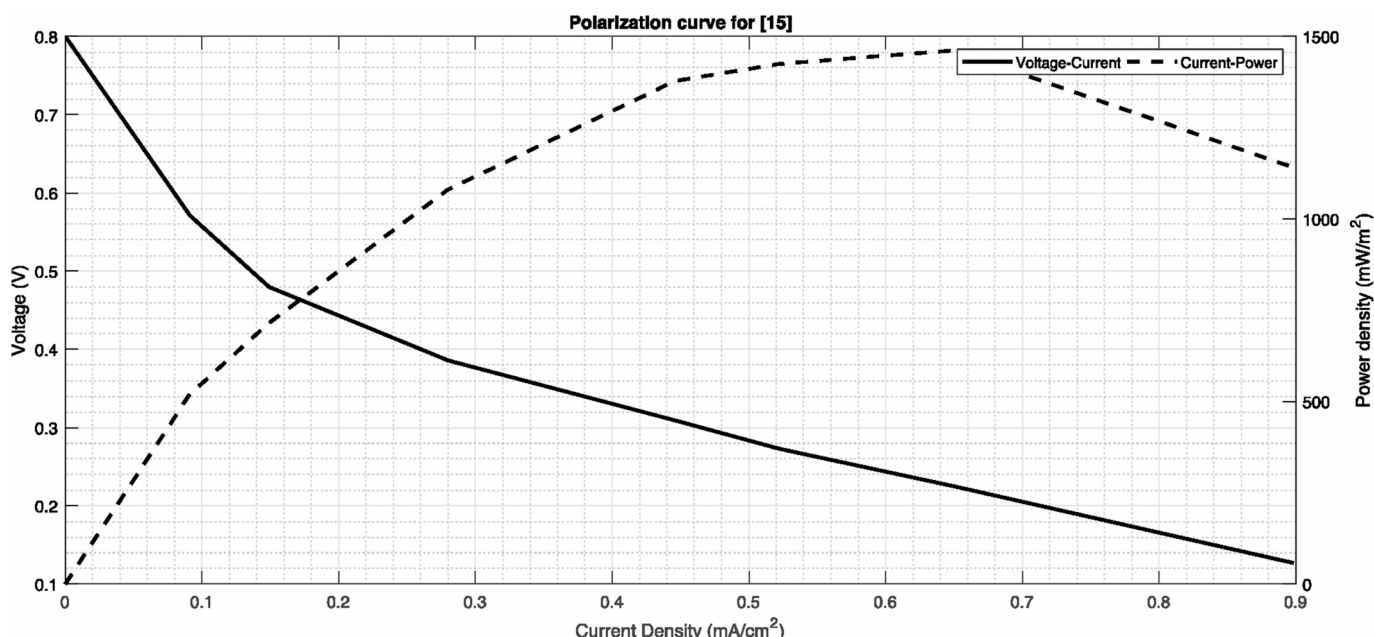


Fig. 21. Polarization curve reconstructed from the data on [15] and the trial with the PVDF cathode.

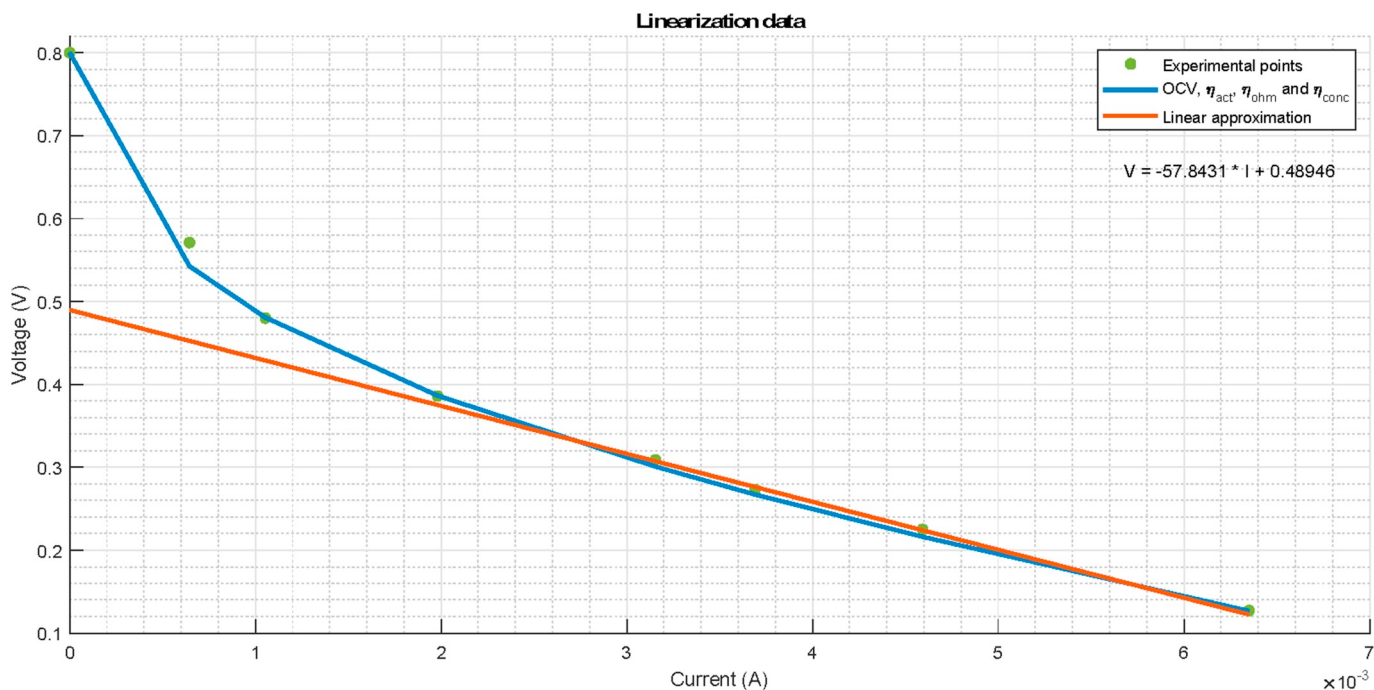


Fig. 22. Linearization procedure for polarization data on [15]. The slope of the linear regression, the internal resistance estimate, is between 50 and 75 Ω .

Table 3

Parameter estimation through GraphPad Prism 7 for non-linear regression and linear regression for internal resistance.

Parameter	Values for non-linear regression	Value for linear regression
A	Fixed at 800×10^{-3} V	
B	1.107×10^{-1}	
B ₁	8.515×10^{-5}	
R	30.62Ω	$\approx 58 \Omega$
C	3.842×10^{-6}	
D	227.3	

The ohmic losses (η_{ohm}) exhibit a linear behavior and can be modeled by the ohm's law:

$$\eta_{ohm} = i \times R_{ohm} \quad (7)$$

Concentration losses can be modeled by:

$$\eta_{conc} = c \times \ln\left(1 - \frac{i}{i_1}\right) \quad (8)$$

The parameter i_1 is a constant that depends on the fuel cell and its operating state. i_1 is used to represent the limiting current at which the fuel is used up at a rate equal to its maximum supply speed. This equation, however, has severe limitations when applied to describe air exposed, batch-fueled, fuel cells, rather than fuel cells exposed to pure oxygen. Low temperature fuel cells are also not adequately described by this equation. Applying these considerations and the same principle as for equation (5), equation (9) outputs a curve that better fits experimental data:

$$\eta_{conc} = c \times e^{d \times i} \quad (9)$$

The contribution of each of the losses accounts for the overall voltage and current measured at an MFC terminal by the equation:

$$V_{OUT} = A_{theory} - b \times \ln\left(\frac{i}{B_1} + 1\right) - i \times R_{ohm} - c \times e^{d \times i} \quad (10)$$

where A_{theory} represents the theoretical open circuit voltage. Considering that during the experimental procedures, the same cathode area and reactor volume was preserved, current densities can be converted to absolute current values, in mA. The open circuit voltage measured will also be different than the theoretical value and equation (10) yields:

$$V_{OUT} = A - B \times \ln\left(\frac{I}{B_1} + 1\right) - I \times R_{ohm} - C \times e^{D \times I} \quad (11)$$

With GraphPad Prism 7 and through the methods previously described, this equation is used as a non-linear regression for the R1 and R2 current-voltage averaged data at 63 inoculation days. Following the methods previously presented, Fig. 16 represents the linear regression for 200, 100 and 68 Ω .

With both the OCV value (variable A) and an upper limit for the R parameter, an assessment for all the variables is now possible. The parameter estimation is summed up in Table 1.

As can be seen by the data on Table 1, the internal resistance of an MFC reactor is more than the ohmic contribution [29]. Approximately half of the contributions to the internal resistance are related with activation and concentration losses. The value found for the total internal resistance is also consistent with the external resistance at which the maximum power was achieved, following the maximum power point theorem [17]. Fig. 17 allows for a clearer representation of the influence and weight of each loss, with the plot in purple representing the sum of the losses, and, therefore, the full steady-state equation.

3.2. Applying the steady-state equation to predict polarization curves

3.2.1. On reactors with the same volume, substrate, bacteria and electrodes

The second set of reactors inoculated – R3 through R6 – was used to determine the validity of the steady-state equation previously determined. To clearly represent all the data points, voltage values belonging to the same polarization trials were averaged and used for comparison purposes. The plots on Fig. 18 clearly show that there were no power overshoot conditions in either trial and that the maximum power of about 880 mW/m² (0.622 mW at 248 mV) was achieved at 43 days and around the same external load, approximately 100 Ω .

Having results so close to the ones used to determine the steady state

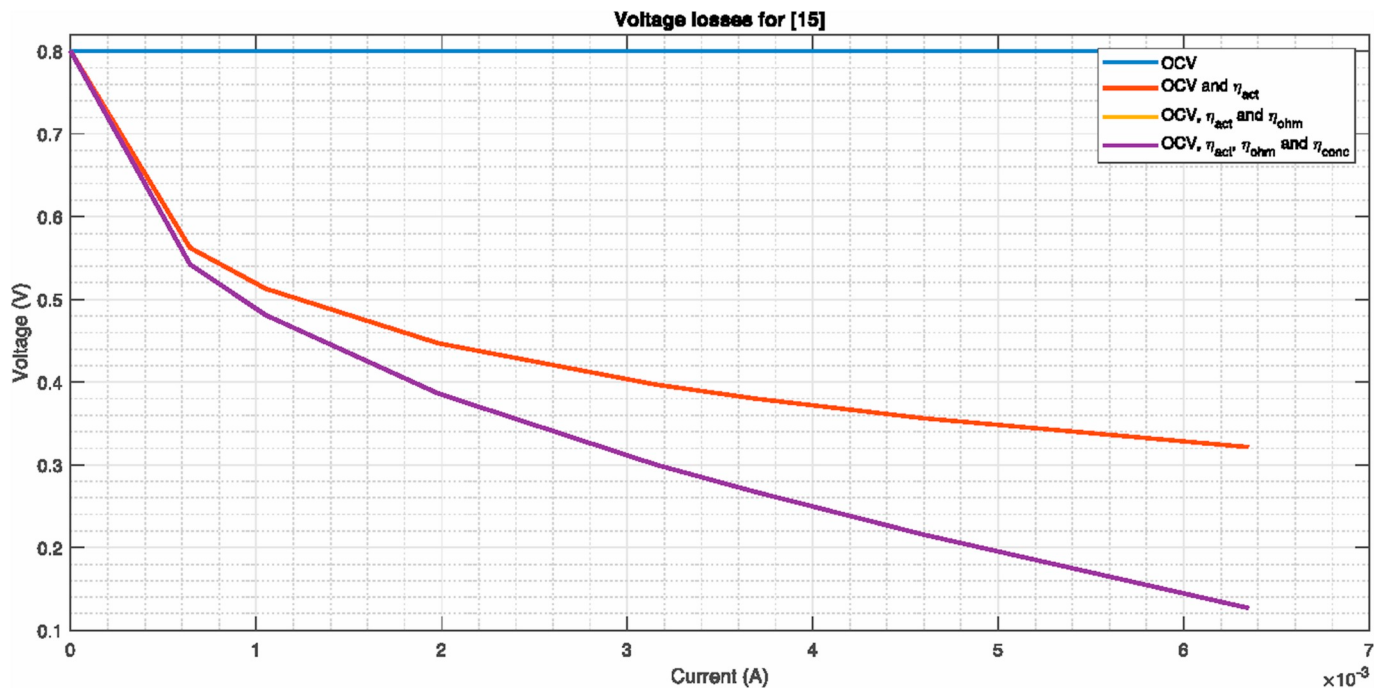


Fig. 23. Voltage losses plot for the polarization data on [15]. The ohmic losses are missing because they are superimposed on the activation losses, meaning they are irrelevant for the particular settings on this reactor.

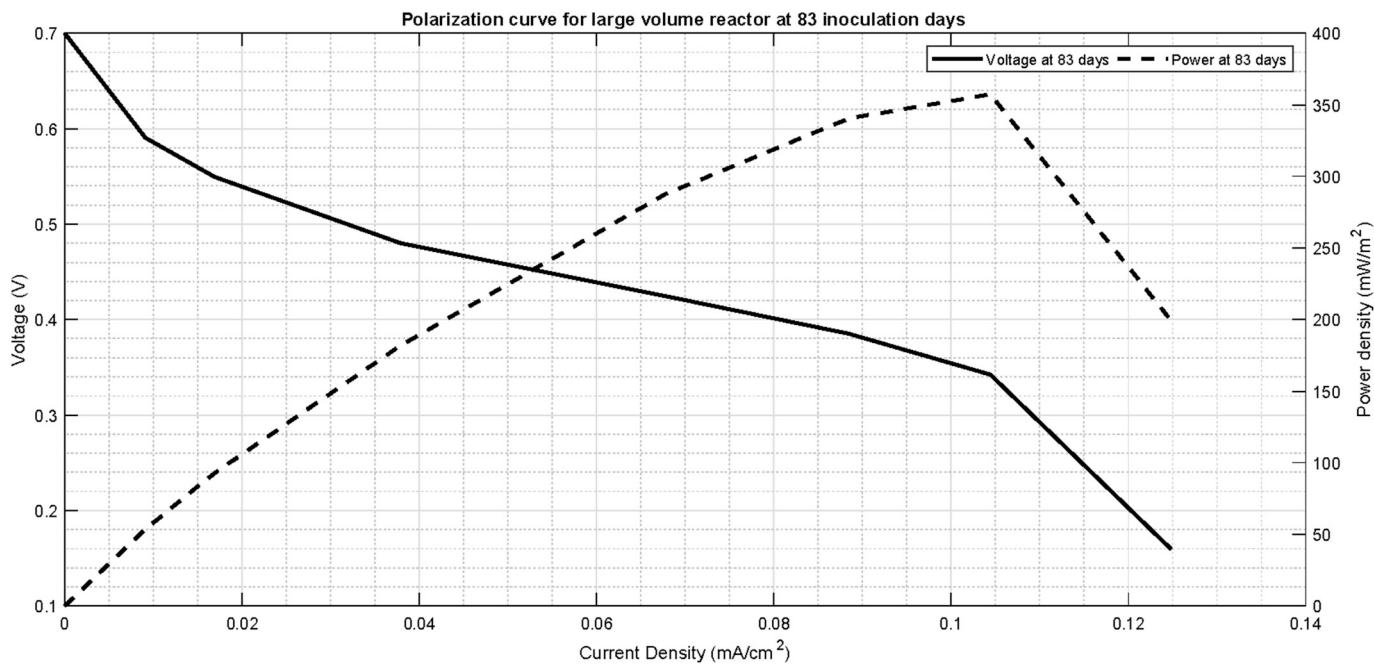


Fig. 24. Polarization curve built from averaged voltage values per hour and external load at 83 inoculation days for a large volume reactor.

equation is a clear indication that similar reactors exposed to similar conditions are expected to have close voltage current profiles, as proved on Fig. 19.

Supported by previous colonization procedures, reactors from the second colonization batch reached higher current densities, although similar voltage levels. Determining the absolute deviation from the steady state equation shows that this standard equation can be used to estimate the voltage current profile from 500 to 68Ω , as shown by Fig. 20.

An accurate calculus of the relative deviation, presented in Table 2,

further reinforces the applicability of the steady-state equation, and what range is safe to use for an electrical model development.

3.2.2. On a reactor from another study, RT1

The work in Ref. [15] is a detailed description of the method applied for producing the activated carbon air-cathode. To validate such procedure and achievement, the research team subjected the electrode to application settings, using it on a 28 mL MFC with the same anode brush and substrate as the one described in this work. The polarization data of RT1 there presented, and here in Fig. 21, was used to apply the described

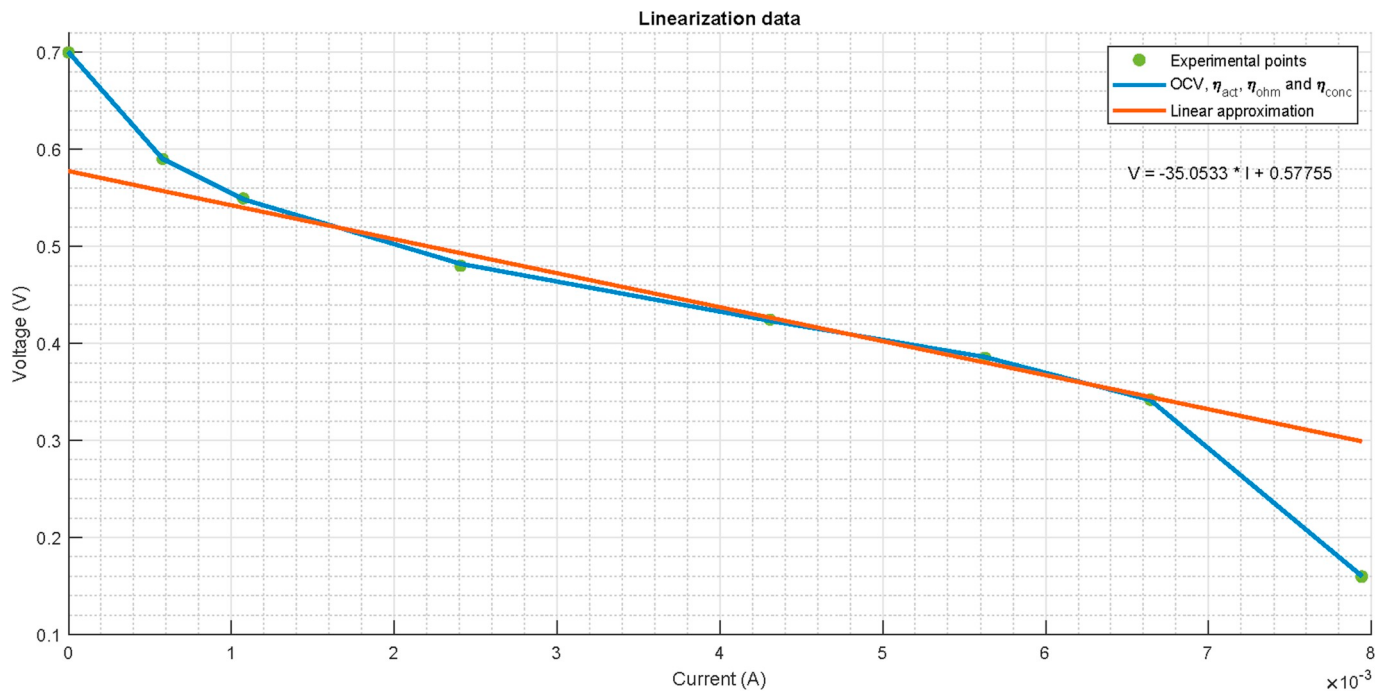


Fig. 25. Linear fit for a large 250 mL reactor and loads between 100 and 51.5 Ω at 84 inoculation days.

Table 4
Parameter estimation for a larger volume equivalent of the small reactors.

Parameter	Values for non-linear regression	Value for linear regression
A	Fixed at 700×10^{-3} V	
B	7.65×10^{-2}	
B ₁	1.98×10^{-4}	
R	8.49Ω	$\approx 35 \Omega$
C	2.906×10^{-6}	
D	1395	

method.

Since the maximum power was reached for 50Ω , two other values in the ohmic region were chosen for the linearization procedure: the voltage-current pairs for 75 and 100Ω .

The slope of the line in Fig. 22 provides a rough estimate for the internal resistance of RT1. Although no information was retrieved on the open circuit voltage of the considered research, an estimate, based on the results for R1 through R6 of this study, of 0.8 V was made. Table 3 presents the result of the non-linear regression on all the equation variables, which is, as expected, over 50Ω and under 75Ω .

The weight of each loss in this polarization trial is exposed with

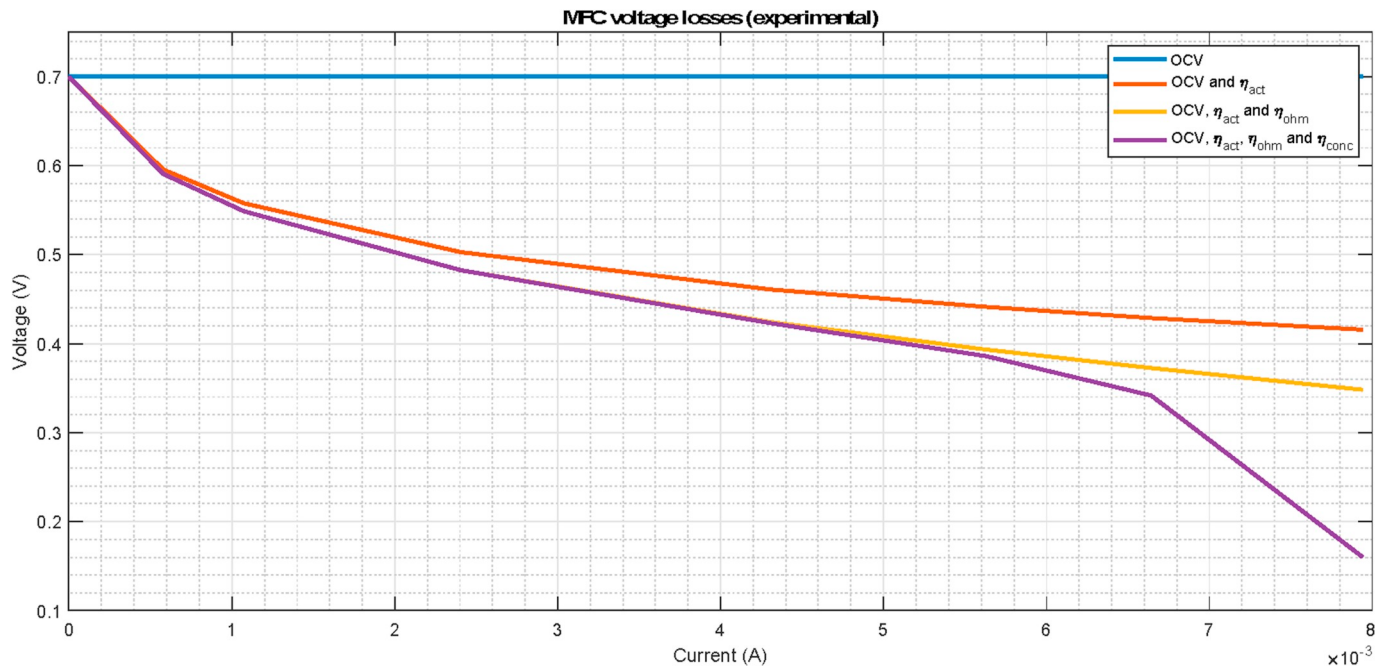


Fig. 26. Voltage losses discrimination according to the estimates for the polarization curve parameters.

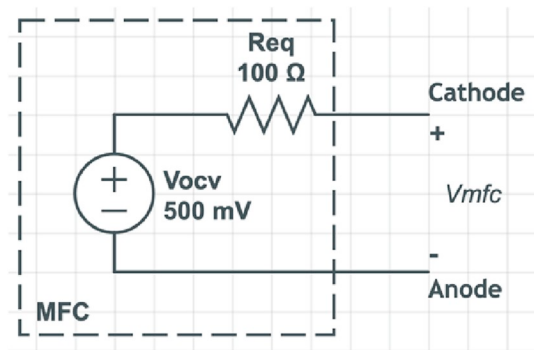


Fig. 27. Electrical model for describing the steady state behavior of a 28 mL single chamber air-cathode microbial fuel cell.

Fig. 23. It can be observed that the ohmic and concentration losses are superimposed, meaning that the concentration losses are neglectable. This means that the flow between reactants (acetate) and products (water) happens without any unbalances, which, in turn, proofs that the biofilm is acclimated even for high currents. Typically, such polarization curves are common between biofilms with over 1 year.

3.2.3. On a larger volume reactor, RT2

The presented method for determining the polarization curve equation was applied to a large volume reactor, RT2, as a further proof of the method feasibility. The data used for method validation was retrieved with a biofilm 84 days old. The polarization data is presented in Fig. 24.

The polarization curve shows a typical behavior, albeit the drop for higher currents. This drop shows that the biofilm still needs more time to develop and achieve full maturation, although ready for polarization trials as no power overshoot is pictured. The maximum power achieved was of 357 mW/m^2 (2.27 mW at approximately 342 mV for 51.5Ω).

Applying the same method as for the small volume reactors, a linear regression, pictured in Fig. 25 was applied to the vicinity of the maximum power point: the voltage-current relationship for 68Ω and 100Ω were selected as the most adequate data points to describe the ohmic region, apart from the pair for the maximum power (51.5Ω). In this particular case, since data between 51.5Ω and 20Ω is missing (as depicted by the sharp drop after 0.10 mA/cm^2), specific measures were needed dimension the polarization equation.

Table 4 presents the estimates for each of the polarization curve unknowns.

By knowing each of the variables weight, a full description of the reactor's losses can be developed, as shown in Fig. 26.

A quick comparison of the internal resistance of the small and large volume reactors hints that the internal resistance of the large reactor is smaller, allowing for the development of larger currents at similar loads. The proportion in volume, however, does not follow the same path: a large volume reactor exhibits smaller power densities although higher in absolute value. Research will follow on this topic supported by the results previously presented and discussed.

3.3. Developing an electrical circuit model from the steady state equation

Considering Table 2 and a generic 28 mL air-cathode, anode carbon brush, acetate substrate reactor, an MFC electrical model can be developed to resistances between 500 and 68Ω . In such range, the polarization curve is mostly described by a linear regression in the following form:

$$V_{mfc} = V_{OCV} - I \times R_{eq} \quad (12)$$

where V_{OCV} represents the measured open circuit voltage and R_{eq} the total value of the internal resistance, as previously discussed. The model, therefore, has an equivalent electric circuit composed of a voltage source

and a 100Ω resistance connected in series. Details on the transient response are out of the scope of this work and the model on Fig. 27 is applied as describing only the steady state behavior of a specific, previously described, MFC.

4. Conclusion

A systematic analysis of a set of 28 mL single-chamber air-cathode reactors, applying the multi-cycle method and artificial wastewater, has shown that the electric behavior of Microbial Fuel Cells can be standardized for steady state conditions. The presented work clearly exposes a method to estimate and predict the internal power losses on MFC reactors without the need for expensive instrumentation devices or intricate numerical methods. The application of this method to other researches and reactor topologies was also addressed and successfully proven. The proposed mathematical model is represented by the serial connection of a 100Ω resistance with a 500 mV DC power source. This outcome provides useful information for designing a DC/DC converter, capable of boosting the voltage level of such a fuel cell, making it a fundamental element of LP and ULP smart-sensors. Such a solution would provide an autonomous and independent quality monitoring tool, which, coupled with adequate communication protocols, could increase measurements accuracy, reliability and frequency, whilst decreasing economical expenses. In itself, using an MFC as a power source, irrespective of its pairing, has been a challenge because of incoherent wastewater composition. A model as the one here proposed will allow for adequate trials with maximum power point tracking algorithms and voltage boosting hardware in order to overcome the previously mentioned challenges for power production. Future work on this topic will follow, by using the proposed methodology for designing energy regulation stages that are capable of managing the use of the harvested power.

Data availability

Datasets related to this article can be found at <https://doi.org/10.17632/zj7ytsrsgj.1>, an open-source online data repository hosted at Mendeley Data ([30]).

Acknowledgments

This work was funded by the Portuguese Foundation for Science and Technology (FCT) (Grant ERANETMED/0004/2014), through the ERANETMED initiative of Member States, Associated Countries and Mediterranean Partner Countries (Project ID eranetmed_nexus-14-044).

Appendix A. Supplementary data

Supplementary data to this article can be found online at <https://doi.org/10.1016/j.rser.2019.109439>.

References

- [1] Helmbrecht J, Maier M, Morillo EM, Kühlers D, Roth K. Improvement of the water-energy nexus and the environmental performance of water supply systems using smart. *ICT Solutions* 2016;11:679–89.
- [2] Espírito-Santo A, Serra P, Albuquerque S, Ribeiro B, Santos F, Páscoa J. Low-power smart sensing in energy and water systems integration. In: 2017 IEEE int. Work. Meas. Networking, M N 2017 - proc.; 2017. <https://doi.org/10.1109/IWMN.2017.8078408>.
- [3] Huang L, Pop V, de Francisco R, Vullers R, Dolmans G, de Groot H, et al. Ultra low power wireless and energy harvesting technologies — an ideal combination. In: 2010 IEEE int. Conf. Commun. Syst. IEEE; 2010. p. 295–300. <https://doi.org/10.1109/ICCS.2010.5686436>.
- [4] Ultra low power wireless connectivity technology backgrounder. n.d., <http://www.nordicsemi.com/eng/News/Press-Center/Press-Backgrounders/ULP-wireless-connectivity-backgrounder>. [Accessed 18 October 2014].
- [5] Raju M, Grazier M. ULP meets energy harvesting: a game-changing combination for design engineers. TI, <http://Focus TI Com/Lit/Wp/Slyy018/Slyy018 Pdf 2008>.

- [6] Bullen RA, Arnot TC, Lakeman JB, Walsh FC. Biofuel cells and their development. *Biosens Bioelectron* 2006;21:2015–45. <https://doi.org/10.1016/j.bios.2006.01.030>.
- [7] Davis F, Higson SPJ. Biofuel cells - recent advances and applications. *Biosens Bioelectron* 2007;22:1224–35. <https://doi.org/10.1016/j.bios.2006.04.029>.
- [8] Lovley DR. Bug juice: harvesting electricity with microorganisms. *Nat Rev Microbiol* 2006;4:497–508. <https://doi.org/10.1038/nrmicro1442>.
- [9] Rabaey K, Rodríguez J, Blackall LL, Keller J, Gross P, Batstone D, et al. Microbial ecology meets electrochemistry: electricity-driven and driving communities. *ISME J* 2007;1:9–18. <https://doi.org/10.1038/ismej.2007.4>.
- [10] Santoro C, Arbizzani C, Erable B, Ieropoulos I. Microbial fuel cells: from fundamentals to applications. A review. *J Power Sources* 2017;356:225–44. <https://doi.org/10.1016/j.jpowsour.2017.03.109>.
- [11] Ortiz-Martínez VM, Salar-García MJ, de los Ríos AP, Hernández-Fernández FJ, Egea JA, Lozano LJ. Developments in microbial fuel cell modeling. *Chem Eng J* 2015;271:50–60. <https://doi.org/10.1016/j.cej.2015.02.076>.
- [12] Recio-Garrido D, Perrier M, Tartakovsky B. Combined bioelectrochemical-electrical model of a microbial fuel cell. *Bioproc Biosyst Eng* 2016;39:267–76. <https://doi.org/10.1007/s00449-015-1510-8>.
- [13] Xia C, Zhang D, Zhu Y, Guo Y. Models for microbial fuel cells : a critical review. 2017. p. 19–20. <https://doi.org/10.1049/joe.2017.0533>.
- [14] Wen Q, Wu Y, Cao D, Zhao L, Sun Q. Electricity generation and modeling of microbial fuel cell from continuous beer brewery wastewater. *Bioresour Technol* 2009;100:4171–5. <https://doi.org/10.1016/j.biortech.2009.02.058>.
- [15] Yang W, He W, Zhang F, Hickner MA, Logan BE. Single-step fabrication using a phase inversion method of poly(vinylidene fluoride) (PVDF) activated carbon air cathodes for microbial fuel cells. *Environ Sci Technol Lett* 2014;1:416–20. <https://doi.org/10.1021/ez5002769>.
- [16] Watson V, Estadt G. Graphite fiber brush anodes for increased power production in Air-Cathode Microbial Fuel Cells 2007;41:3341–6.
- [17] Domingos Serra PM, Esorito-Santo A, Magrinho M. Energy harvesting from wastewaters with a single-chamber air-cathode microbial fuel cell. In: Iecon 2018 - 44th annu. Conf. IEEE Ind. Electron. Soc., vol. 31. IEEE; 2018. p. 3847–51. <https://doi.org/10.1109/IECON.2018.8592827>.
- [18] Kim JR, Min B, Logan BE. Evaluation of procedures to acclimate a microbial fuel cell for electricity production. *Appl Microbiol Biotechnol* 2005;68:23–30. <https://doi.org/10.1007/s00253-004-1845-6>.
- [19] Watson VJ, Logan BE. Analysis of polarization methods for elimination of power overshoot in microbial fuel cells. *Electrochim Commun* 2011;13:54–6. <https://doi.org/10.1016/j.elecom.2010.11.011>.
- [20] Zhao F, Slade RCT, Varcoe JR. Techniques for the study and development of microbial fuel cells: an electrochemical perspective. *Chem Soc Rev* 2009;38:1926. <https://doi.org/10.1039/B819866g>.
- [21] Zhang P-Y, Liu Z-L. Experimental study of the microbial fuel cell internal resistance. *J Power Sources* 2010;195:8013–8. <https://doi.org/10.1016/j.jpowsour.2010.06.062>.
- [22] Yang F, Zhang D, Shimotori T, Wang K-C, Huang Y. Study of transformer-based power management system and its performance optimization for microbial fuel cells. *J Power Sources* 2012;205:86–92. <https://doi.org/10.1016/j.jpowsour.2012.01.025>.
- [23] Logan BE, Hamelers B, Rozendal R, Schröder U, Keller J, Freguia S, et al. Microbial fuel cells: methodology and technology †. *Environ Sci Technol* 2006;40:5181–92. <https://doi.org/10.1021/es0605016>.
- [24] Logan BE. Microbial fuel cells. Hoboken, NJ, USA: John Wiley & Sons, Inc.; 2007. <https://doi.org/10.1002/9780470258590>.
- [25] Niemann J. Unraveling fuel cell electrical measurements. 2004. p. 1–6. <https://www.google.com/url?sa=t&rct=j&q=&esrc=s&source=web&cd=2&ved=2ahUKEwjTpqPYlqvAhWyo3EKHKF-AnwQFjABegQIAxAC&url=https%3A%2F%2Fwww.tek.com%2Fdocument%2Ftechnical-article%2Funraveling-fuel-cell-electrical-measurements&usg=AOvVaw39P3oMDY6wdRZ-VetPFMDU>.
- [26] Logan BE. Essential data and techniques for conducting microbial fuel cell and other types of bioelectrochemical system experiments. *ChemSusChem* 2012;5: 988–94. <https://doi.org/10.1002/cssc.201100604>.
- [27] Hong Y, Call DF, Werner CM, Logan BE. Adaptation to high current using low external resistances eliminates power overshoot in microbial fuel cells. *Biosens Bioelectron* 2011;28:71–6. <https://doi.org/10.1016/j.bios.2011.06.045>.
- [28] Rossi R, Yang W, Zikmund E, Pant D, Logan BE. In situ biofilm removal from air cathodes in microbial fuel cells treating domestic wastewater. *Bioresour Technol* 2018;265:200–6. <https://doi.org/10.1016/j.biortech.2018.06.008>.
- [29] Fan Y, Sharbrough E, Liu H. Quantification of the internal resistance distribution of microbial fuel cells. *Environ Sci Technol* 2008;42:8101–7. <https://doi.org/10.1021/es801229j>.
- [30] Serra PMD. Polarization data for 28 mL MFC reactors. 2019. <https://doi.org/10.17632/zj7ytsrsrgj.1>.